Spring 2016

Apatite Helium Thermochronology of the Blue Nile Canyon, Ethiopian Plateau

Nathaniel C. Blackburn
Western Kentucky University, nathaniel.blackburn298@topper.wku.edu

APATITE HELIUM THERMOCHRONOLOGY OF THE BLUE NILE CANYON, ETHIOPIAN PLATEAU

A Thesis
Presented to
The Faculty of the Department of Geography and Geology
Western Kentucky University
Bowling Green, Kentucky

In Partial Fulfillment
of the Requirements for the Degree
Master of Science

By
Nathaniel C. Blackburn

May 2016

APATITE HELIUM THERMOCHRONOLOGY OF THE BLUE NILE CANYON, ETHIOPIAN PLATEAU

Date Recommended 3/15/2016

Dr. Nahid Gani, Director of Thesis

Dr. Aaron Celestian

Dr. Xingang Fan

3/21/16

Dean, Graduate Studies and Research Date

ACKNOWLEDGMENTS

I would like to thank my advisor Dr. Nahid Gani for her guidance, motivation and patiently working with me throughout this research project, and graduate studies. I would also like to thank my committee members, Dr. Aaron Celestian and Dr. Xingang Fan, for their critical comments and suggestions to improve this thesis project. Thanks are due to Dr. Matthijs van Soest for his work and contribution to the apatite helium dating used in this project. I would also like to thank Alexander Falster and Prabhat Neupane of the Earth and Environmental Sciences at the University of New Orleans for providing me the opportunity to use their geochemistry lab facilities for sample preparation. I would like to thank Omni Gipson, Charlye Jackson, Red Blackburn, and Fred Noe for editing assistance and technical support. Kibre Tadese of the Ethiopian Geological Survey is greatly acknowledged for his assistance in the field during sample collection. This project was partially supported by the National Science Foundation Geomorphology and Landuse Dynamics program (grant EAR-0964876), Louisiana Board of Regents (LEQSF (2010-13)-RD-A-17), and Western Kentucky University (WKU) Research and Creative Activities I (RCAP I-14-8056) grants to Dr. Gani. I would also like to thank the WKU Department of Geography and Geology for providing graduate assistantship and travel funding to support this research. Thanks are also due to the Geological Society of America On To the Future (OTF) and WKU Graduate School for travel funding, and Veterans Affairs for additional support.

CONTENTS

LIST OF FIGURES

LIST OF TABLES

APATITE HELIUM THERMOCHRONOLOGY OF THE BLUE NILE CANYON, ETHIOPIAN PLATEAU

Nathaniel C. Blackburn May 2016 55 Pages

Directed by: Dr. Nahid Gani, Dr. Aaron Celestian, and Dr. Xingang Fan

Department of Geography and Geology Western Kentucky University

The Ethiopian Plateau, situated in the northernmost part of the East African Rift System, has been uplifted and incised by the Blue Nile River, creating the 1.5 km-deep Blue Nile Canyon, the only extensive canyon within the Nile drainage basin. Much of this canyon incision is related to the Ethiopian Plateau uplift, which is due to a combined tectonic influence linked to the East African Rift System and the Afar Mantle Plume-related upwelling since the Oligocene. The Blue Nile Canyon incision followed this plume-related upwelling, which resulted in extensive flood basalt emplacement around ~30 Ma. This study employs low-temperature apatite (U-Th)/He thermochronology to better understand the timeline and mode of the Blue Nile Canyon incision and the landscape geodynamics of the Ethiopian Plateau. Neoproterozoic basement rocks and Mesozoic sedimentary rock samples were collected in a vertical transect along the Blue Nile Canyon for AHe dating. Euhedral apatite grains that are inclusion-free and fractureless were selected for dating. The Australian Scientific Instrument (ASI) Alphachron and Inductively Coupled Plasma Mass Spectrometer (ICP-MS) measured the concentrations of radiogenic isotopes uranium (U), thorium (Th), and helium (He) to obtain apatite helium (AHe) dates, providing (U-Th)/He cooling ages ranging from 64 to 460 Ma. These AHe dates are much older than the 30 Ma flood basalt event, thus older than the canyon incision. In this study, a cooling/thermal history is suggested by explaining the data dispersion by the radiation damage effect in the dated apatite grains,

which is related to He retention with time. The apatite suite has been subjected to protracted cooling, longer residence time in the He partial retention zone, and partial resetting due to Mesozoic rift-related burial and subsidence from deposition of ~1.2 km-thick sedimentary rocks, the extensive emplacement of ~1 km-thick flood basalt at 30 Ma, and differential incision. Radiation Damage Accumulation and Annealing Model (RDAAM) time-temperature thermal models indicate a rapid cooling event, suggesting rapid incision after 10 Ma, which is explained by an increase in uplift of the Ethiopian Plateau, likely due to mantle delamination.

CHAPTER 1: INTRODUCTION

1.1. Discussion of Research

The Ethiopian Plateau has undergone uplift and incision associated with the East African Rift System and Afar Mantle Plume. Plateau incision in a continental extension setting undergoing dynamic uplift is rare in the literature, and thus is poorly understood. The Ethiopian Plateau in the proximity of the East African Rift system experienced a total of ~2 km uplift during the Cenozoic (e.g., Gani et al., 2007). Upwelling of the Afar mantle plume and lithospheric flexure of the flanks related to this rifting has contributed to the rise of the Ethiopian Plateau (Beyene and Abdelsalam, 2005; Collet et al., 1999; Gani et al., 2007; Moucha and Forte, 2011; Pik et al., 2003). The Ethiopian Plateau is the northwesternmost part of the East African Rift System that is dissected by the Main Ethiopian Rift into the northwestern plateau and the southeastern plateau (Figure 1.1). As the plateau gained ~2 km elevation (Gani et al., 2007; Pik et al., 2003), the incision by the Blue Nile River and its tributaries on the northwestern plateau formed the 1.5 km-deep Blue Nile Canyon, the only extensive canyon in the greater Nile drainage basin. The incision of the Blue Nile River also exhumed the overlying Quaternary, Miocene-Pliocene volcanic rocks and Cenozoic flood basalts at 30 Ma (Hofmann et al., 1997) to expose the thick accumulation of Mesozoic sedimentary rocks and Neoproterozoic basement rocks. Although the plateau is characterized by the presence of ~500 km-wide low-velocity zone (Bastow et al., 2008) related to the rising of the Afar mantle plume, there is no consensus on the timing of the plateau incision (particularly after the 30 Ma

flood basalt eruption) or the uplift of the plateau (Gani et al., 2007; Pik et al., 2003; 2008; Quade and Wynn., 2008).

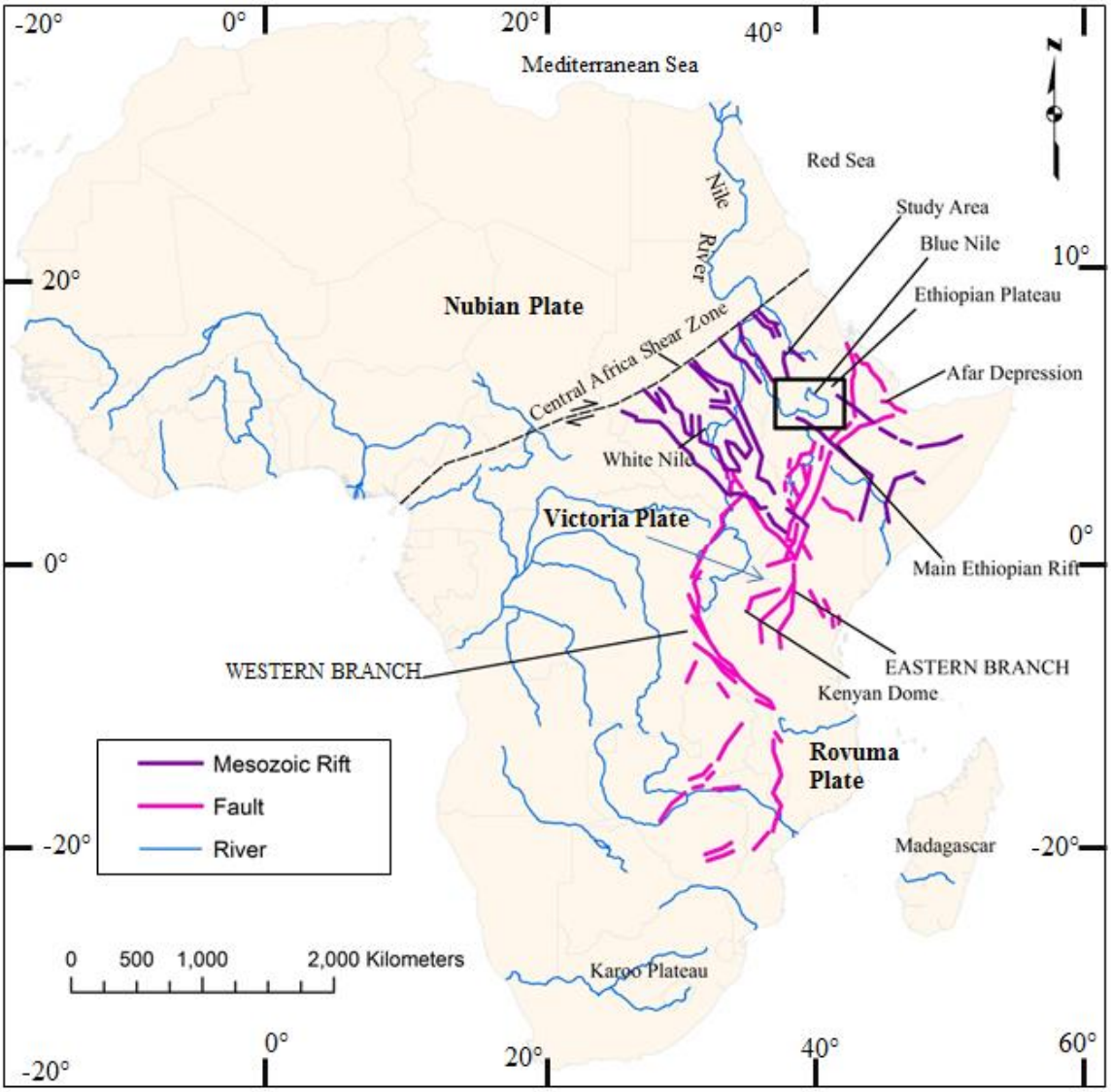

Figure 1.1: Tectonic map of the East African Rift System. Note NW-SE trending Mesozoic rifting (purple lines) superimposed by NE-SW trending Miocene rifting (pink lines). The two main branches, Western and Eastern Branch of the Miocene rifting are shown. Note the Precambrian Central African Shear Zone bounding the northwestern limit of the Mesozoic rifts. Blue lines indicate major rivers in Africa. The study area is indicated by the black rectangle, which includes the Ethiopian Plateau and the Blue Nile.

After exiting the plateau, the Blue Nile joins the White Nile to become the main Nile River, which drains to the Mediterranean Sea

Source: Modified from Corti, 2009; Gani et al., 2009.

The timing of the Ethiopian Plateau elevation gain has been contested. Some inferred that the plateau was uplifted in the upper Eocene (e.g., Beydoun, 1960). However, later works have indicated an Oligocene uplift, with some suggesting an early (before 20 Ma) (Pik et al., 2003; 2008) and others arguing a late (after 10 Ma) rise of the Ethiopian Plateau (Adamson and Williams, 1987; Gani et al., 2007; Gani, 2015). To understand the most recent uplift history (within a few kilometers of the surface), low-temperature thermochronology has been widely utilized for cooling or thermal history, particularly during exhumation. Thermochronological investigations using the minerals apatite and titanite in aliquots have been conducted on the Ethiopian Plateau (Pik et al., 2003; 2008). The aliquot apatite (U-Th)/He study of the Blue Nile Canyon (Pik et al., 2003) yielded AHe ages between 45 and 107 Ma, displaying a trend of younger AHe age with increasing elevation that was interpreted as partial thermal resetting due to burial by the 30 Ma flood basalt. These thermochronological works suggest a rather simple cooling history and steady erosion rate of the Ethiopian Plateau since 25-30 Ma. Gani et al. (2007) and Gani (2015) suggested an increased canyon incision around 10 Ma from quantitative geomorphology and geochronology based studies, and argued for an episodic uplift of the plateau and that much of the ~2 km uplift had occurred around the same time. Thus, the complex tectonic history of the Ethiopian Plateau, including differential uplift events since 30 Ma (Gani et al., 2007; Quade and Wynn, 2008) related to upwelling of the Afar mantle plume and lithospheric flexure of the Main Ethiopian Rift, may not

support a simple thermal or cooling history of the region (Gani et al., 2007; Philippon et al., 2014).

1.2. Objectives and Broader Significance

To better confine the cooling history of the Ethiopian Plateau, this study uses single grain apatite (U-Th)/He thermochronology of the Blue Nile Canyon to understand low temperature thermal history of rocks in the near-surface thermal field (e.g. Braun, 2005; Ehlers and Farley, 2003) as it exhumes the upper 1-3 km within the crust. There is no previous study using single grain AHe dates to understand thermal history of the Ethiopian Plateau. This study extracted AHe dates from single grains that show a wider and anomalous distribution of AHe ages. Previous studies showed that single grain (as opposed to the aliquots of Pik et al., 2003; 2008) AHe ages may have significant data dispersion (e.g., Fitzgerald et al., 2006; Flowers and Kelley, 2011). In such cases, caution should be made for accurate interpretation of thermal history from these single grains' data dispersion. Data dispersion can be a function of He diffusivity (Flowers et al., 2009), He implantation (Fitzgerald et al., 2006; Spiegel et al., 2009) from neighboring U and Th rich phases, grain size variation (Reiners and Farley, 2001), or U and Th zonation (e.g. Fitzgerald et al., 2006). However, recent studies suggest dispersed AHe ages depend on radiation damage and effective uranium concentration in grains (e.g. Green et al., 2006; Shuster et al., 2006; Flowers and Kelley, 2011) that can be explained by reasonable geologic constraints through extracting possible thermal history using the RDAAM (Radiation Damage Accumulation and Annealing Model) of a region (Ault et al., 2009; Flowers et al., 2009; Shuster and Farley, 2009; Flowers and Kelley, 2011).

Thus, the objective of this study is to investigate fundamental causes of the AHe date dispersion and to explain how these concepts can account for the cooling and thermal history related to the Ethiopian Plateau incision. Determining the appropriate cooling history of the Ethiopian Plateau is significant for a better understanding of the exhumation (e.g., uplift), tectonics, geologic processes, and geodynamics of continental rifting (Davidson and Rex, 1980; Ebinger et al., 1989; Bonini et al., 2005; Ebinger, 2005; Corti, 2009; Dugda et al., 2007).

CHAPTER 2: GEOLOGIC OVERVIEW

2.1. General Tectonic Summary of the East African Rift System

The ~6,000 km-long East African Rift System is the largest continental rift system in the world (Chorowicz, 2005; Gani and Gani 2008), extending from the Afar Depression, a rift-rift-rift triple junction between the Main Ethiopian Rift, the Red Sea, and the Gulf of Aden in the north to the Karoo Plateau (Chorowicz, 2005) in the south (Figure 1.1). In the extensional tectonic setting of the South African region, rifting continues as the Rovuma Plate travels east with the Somali plate (Stamps et al., 2008). Just north, in the area of the Kenya Rift, the Victoria plate (Figure 1.1) is also separating from the Nubian plate and travelling east toward the Somali plate (Corti, 2009; Flowers and Schoene, 2010).

According to the most recent studies (Gani et al., 2007; Corti, 2009; Pik et al., 2003; 2008), the East African Rift was formed from two main events. Figure 2.1 shows a summary of the tectonic events associated with the development of various segments of the East African Rift. Upwelling at the core-mantle boundary beneath southern Africa initiated the rise of material through the mantle, in a northeast direction, causing lithospheric thinning (<25 km) in present-day East Africa (Pasyanos and Nyblade, 2007). Here, the initial rifting during Miocene to Pliocene began at the Main Ethiopian Rift (Figure 2.1), between the Somali and Nubian plates (Corti, 2009). The rifting was characterized by periodic extension separated by periods of relative stillness (Corti, 2009). Massive flood basalts ensued from 30 Ma, in conjunction with or following the crustal deformation—two dome features, the Kenyan Dome and the Ethiopian Plateau (Pik et al., 2003).

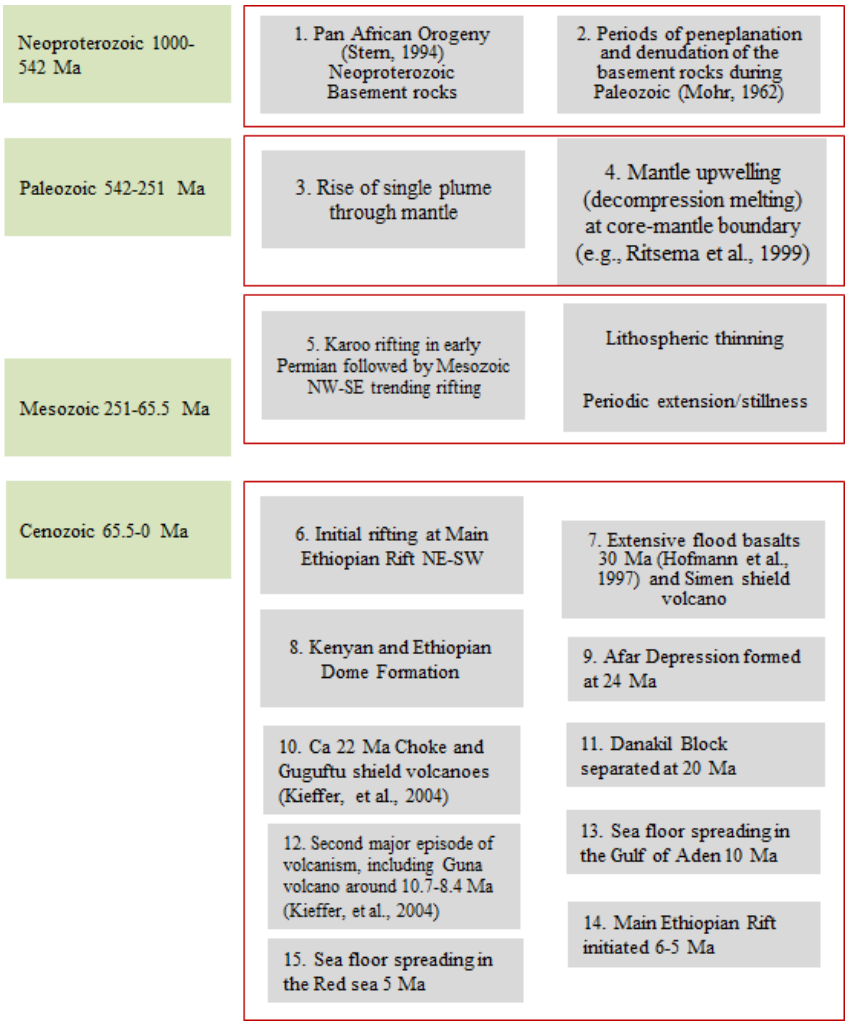

Figure 2.1: Tectonic events within the East African Rift System. In summary, upwelling at the core-mantle boundary triggered lithospheric thinning, and initial rifting began around 30 Ma. Massive flood basalts ensued and formed the Kenyan and Ethiopian Domes. Following uplift and surface motion of the Ethiopian Plateau, there was a shift from NE-SW rifting to NW-SE rifting, which resulted in enhanced topographic relief and increased erosion. Fluvial incision and mass wasting occurred, causing reduced gravitational stress, which led to further tectonic motion.

The Kenya rift lies south of the Afar Depression, below the Main Ethiopian Rift. The region is characterized by low upper mantle velocity and a thin lithosphere. Keller et al. (1994) suggested high velocity in the lower crust and no major seismic anomalies in

the upper crust, implying pervasive magmatism. The initial rifting and volcanism developed along a preexisting ESE-WNW weakness plane from recent Somali-Nubian plate extension, and was rather abrupt, happening within five million years and concentrated around 30 Ma (Corti, 2009). This event produced the main rift valleys, uplifted plateaus, rift depression, subsidence, and development of basins. At this time, the upper stratigraphic flood basalts were deposited, along with lesser rhyolites, tuffs, etc.

The second Pleistocene rifting phase was characterized by volcanism being centralized to the interior of the rift and becoming absent from the plate boundaries, as extension and lithospheric thinning continued, and the rifting progressively evolved towards that characteristic of mid-ocean ridges (Corti, 2009). The Ethiopian Plateau and the Somali Plateau, now separated by the Main Ethiopian Rift Valley, were once united as the Ethiopian Dome or the Ethiopian Plateau (Figure 2.2). As the Main Ethiopian Rift expanded, the two plateaus grew further apart to their current location (Corti, 2009). Numerous volcanic rocks have been deposited on the Ethiopian Plateau, including trachytes, porphyritic basalts, aphyric basalts, and migmatites. On both sides of the Main Ethiopian Rift, 700-2000 m thick volcanic rocks were accumulated with the two major events, the Geba Basalts of 40-32 Ma and Welega Shield Volcanics of 7-15 Ma. The 30 Ma flood basalt deposited ~1 km of material on the Ethiopian Plateau and extended as far as Yemen (Berhe et al., 1987).

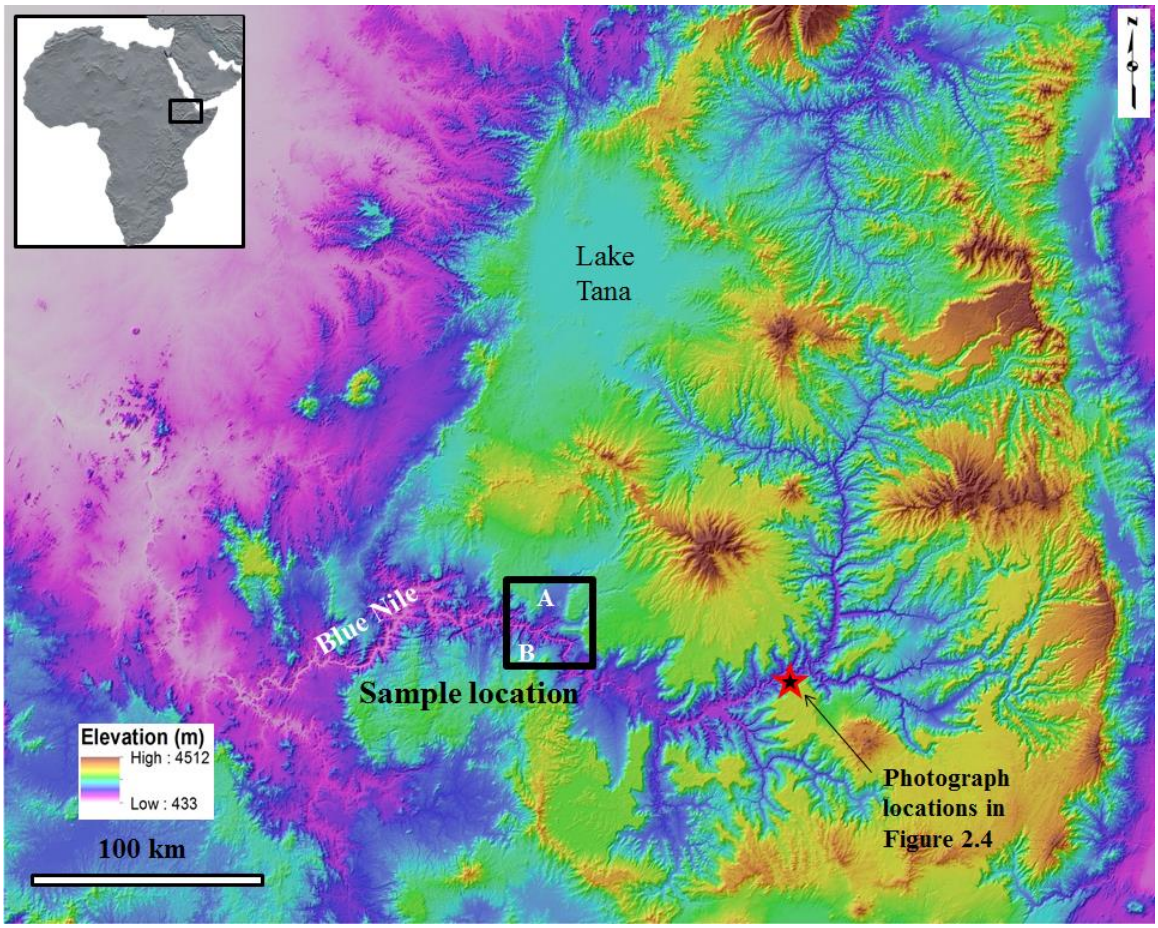

Figure 2.2. Hillshade DEM of the Ethiopian Plateau. This figure displays the hillshade image generated from Shuttle Radar Topography Mission digital elevation model (DEM) data showing the Blue Nile River Canyon of the Ethiopian Plateau, located in East African Rift System. The study area location is shown by the black square. The Ethiopian Plateau is a vast topographic feature of continuous high elevation ranging from 1500 to 4500^{+} m adjacent to the East African Rift on the Nubian (African) Plate. This continental rift is currently active and is attributed to the underlying Afar Mantle Plume.

A more recent study involving fault kinematics, fault gouge and apatite fission-track dating, and slope-area analysis has been executed to better understand the tectonic relationship between the Main Ethiopian Rift and the Kenyan Rift. This work has

proposed a northward spread of rifting, starting in Kenya and propagating to the Main Ethiopian Rift (Philippon et al., 2014).

2.2. Study Area-The Ethiopian Plateau

The Ethiopian Plateau lies near the northern extent of the East African Rift system, adjacent to the Afar Depression, and the Main Ethiopian Rift (Figure 1.1). Due to the rift flank uplift of the Western Escarpment of the Main Ethiopian Rift and mantle plume-related uplift, the plateau is a vast uplifted feature averaging 2km in elevation. A complex tectonic history has developed as the East African Rift has ruptured the African continent over time. The Western Escarpment of the Main Ethiopian Rift, which lies at the eastern extent of the Ethiopian Plateau, was displaced upward due to lithospheric flexure during the opening of the rift. In the Ethiopian Plateau region, Mesozoic rifting associated with rifts trending NW-SE were succeeded by Miocene-Pliocene rifting that generated rifts of NE-SW trends. Various techniques have been employed to understand the active tectonic processes in this region (Pik et al., 2003; 2008; Gani and Gani, 2008; Gani et al., 2007; 2009; Corti 2009; Moucha and Forte, 2011)

Situated within the Ethiopian Plateau, the Blue Nile River (Figure 3) drains from Lake Tana, which lies at around 1,700 m elevation (Henricksen, 1986). The Blue Nile has incised a deep canyon, roughly 1 km deep (Figure 2.3), and exits the plateau to the west (Gani et al., 2007). The Blue Nile then travels to the lowlands of Sudan, where it connects with the White Nile to become the main Nile River, which continues north until it drains into the Mediterranean Sea. At this location, the Nile deposits its sediment load, forming the Nile River Delta. Ninety-six percent of the Delta's sediment originates from

the incision of the Ethiopian Plateau by the Blue Nile River system (Garzanti et al., 2006; Gani et al., 2007).

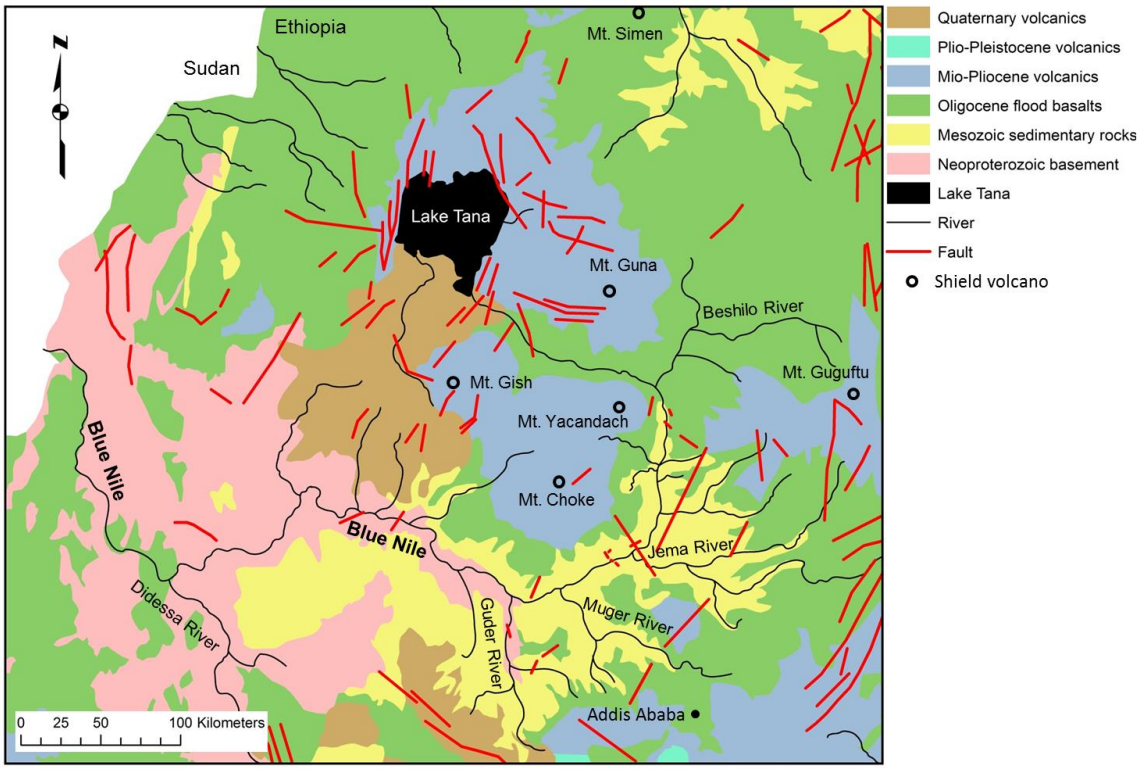

Figure 2.3: Geologic map of study area. The Neoproterozoic basement is overlain by the Mesozoic sedimentary units and several younger volcanic rocks from 30 Ma to present. Note the Blue Nile's deep incision through the volcanic rocks, sedimentary rocks, and into the basement rocks. The Blue Nile River leaves Lake Tana on the Ethiopian Plateau to join the White Nile at Khartoum, Sudan, to form the Greater Nile River. The sediment carved from the Ethiopian Plateau forms the majority of the alluvial fans, Nile Delta, and the Nile Deep Sea Fan.

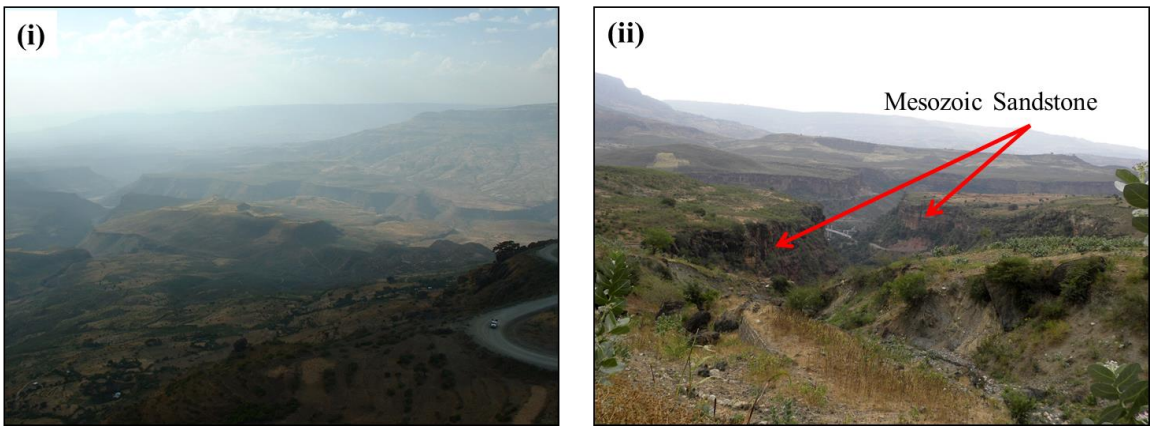

Figure 2.4: Field photographs of the Blue Nile Canyon: (i) Bird's eye view of the Blue Nile Canyon, Ethiopian Plateau; (ii) The Blue Nile incised deeply into the Mesozoic lower sandstone. The location of these field photographs is shown in Figure 2.2.
Source: Photos by Nahid Gani.

Recent works indicate the Blue Nile incision initiated just after the 30 Ma flood basalt, which covered the existing landscape. This new incision resulted in the Tekeze and Blue Nile Rivers being established by 23 Ma (Gani et al., 2007; Pik et al., 2008; Gani, 2015). A previous study by Gani et al. (2007) suggested a three-phase incision, with incision beginning at 30 Ma and increasing in magnitude around 10 Ma and 6 Ma. With these complex faultings, multiple rifting events, and with the uplift and burial events, a complex geological history is left to unravel. In addition, a morpho-tectonic analysis of the Tekeze River and Blue Nile drainage systems suggested three major tectonic/geologic events affecting the incision rate. It began with rising of the Afar mantle plume, causing low to moderate incision around 30 Ma, followed by a buildup of shield volcanoes at 22 Ma. This caused a localized increase in the incision rate around these volcanoes. A third event due to rift-flank uplift of the western escarpment of the Afar Depression at 11 Ma caused a significant increase of the incision rate (Ismail and Abdelsalam, 2012) This activity resulted in the 30 Ma-thick pile of continental flood

basalts found in the upper stratigraphy of the Ethiopian Plateau (Marty et al., 1996; Pik et al., 2003; 2008).

The Ethiopian Plateau exhibits a stratigraphy (Figures 2.3 and 2.4) of various volcanic, sedimentary, and metamorphic sequences. According to Gani et al., (2009), the major stratigraphic unit of the Ethiopian Plateau includes these units from stratigraphically older to younger age: (1) Neoproterozoic basement rocks related to the Pan African Orogeny (Stern, 1994); (2) Triassic-early Jurassic Lower Sandstone. These sandstones unconformably overlie Neoproterozoic basement rocks, which comprise metamorphic rocks and igneous intrusions; (3) Early–Middle Jurassic Upper Limestone unit and Early Jurassic marine glauconitic unit; (4) Late Jurassic–Early Cretaceous Upper Sandstone unit; and (5) a Cenozoic Trap Series consisting of mostly flood basalts with subordinate lava flows, trachyte and rhyolite that dominate the Ethiopian Plateau. These volcanics are covered in places with unconsolidated sediments (Russo et al., 1994).

CHAPTER 3: METHODS

As part of a larger project, samples were collected, apatite grains were separated, and (U-Th)/He thermochronologic dating were conducted (Gani et al., 2011). Several steps are taken prior to (U-Th)/He thermochronologic dating, which are briefly summarized below (Figure 3.1):

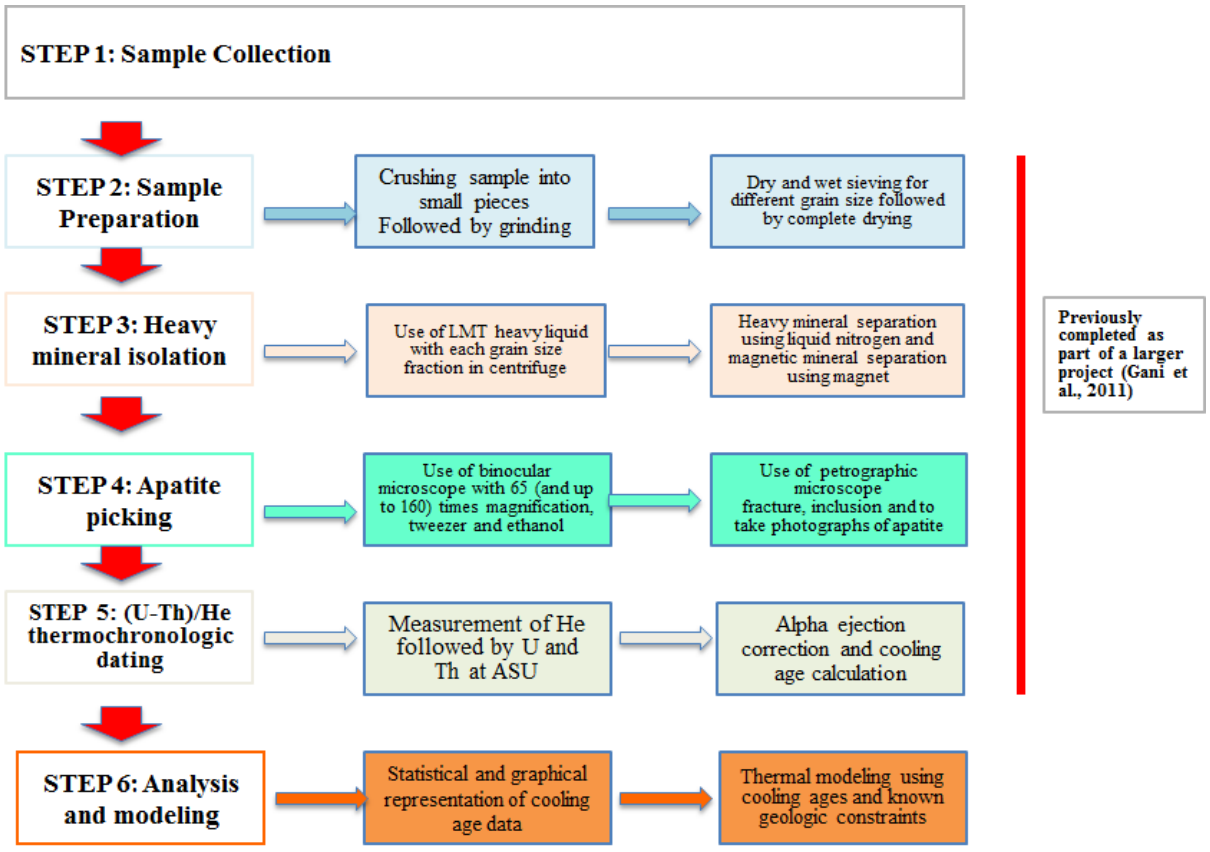

Figure 3.1: Methodological steps for apatite (U-Th)/He dating. Step 6, Analysis and modeling, was the focus of this project. Steps 1-5 were completed previously as part of a larger project.

3.1. Sample Collection

The Blue Nile River has carved a 1.5 km deep incision into the Ethiopian Plateau. Samples were collected from a vertical transect of the Blue Nile Canyon (Figure 3.2). Eight unweathered samples (Figure 3.3) were obtained from the base of the canyon, with each sample site increasing in elevation from 791 to 2022 meters. Seven samples were collected from igneous and metamorphic basement rocks, and two samples from the overlying Triassic/Jurassic sandstone. Note that samples were collected far enough below the 30 Ma flood basalt contact to avoid any effects of possible direct-heating of the basement rocks due to flood basalt emplacement.

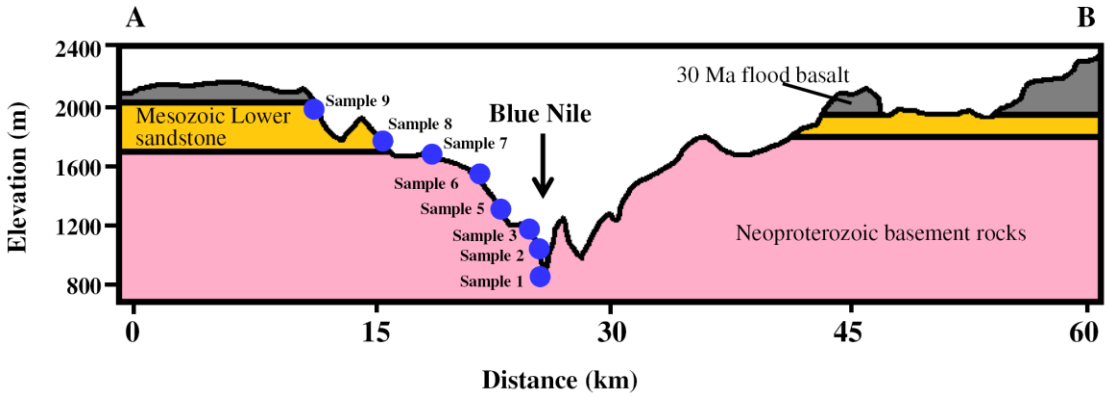

Figure 3.2: Sample profile. Samples were collected from a vertical transect of the Blue Nile Canyon within the Ethiopian Plateau (A-B geologic cross-section location is shown in Figure 2.2). Six samples were collected from the Neoproterozoic granite, and two samples from Mesozoic sandstone. Sample 4 was collected, but contained no apatite grains; therefore, it is not shown. The average 0.5 km-thick 30 Ma flood basalt is shown by the grey color.

Source: Created by the author.

3.2. Sample Preparation

In preparation, each sample was first crushed into a number of large pieces with a sledge hammer, and then crushed further using a tabletop jaw crusher machine to reduce them to finer sediments. The samples were then dry and wet sieved, and separated by grain size ranging from >63µm to >500 µm. The samples were then dried completely, and placed into labeled centrifuge tubes for heavy mineral separation.

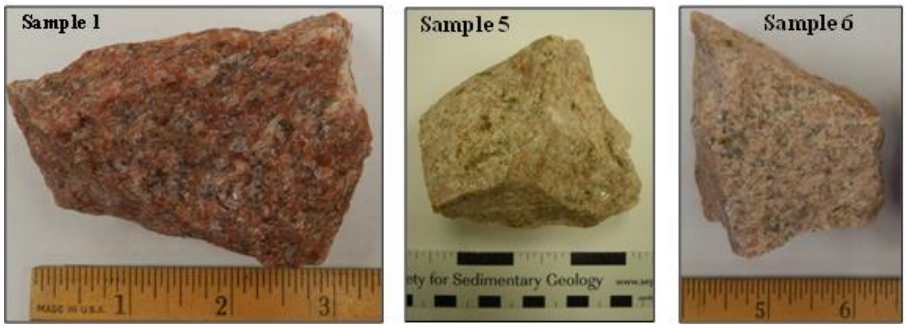

Figure 3.3: Photographs of samples. Displayed are examples of a few samples collected from the vertical transect of the Blue Nile Canyon within the Ethiopian Plateau.
Source: Photos by Nahid Gani.

3.3. Heavy Mineral and Magnetic Mineral Separations

Heavy mineral separation is performed to isolate the heavy minerals from the light minerals. Each sample is submerged in Lithium Metatungstate heavy liquid in a test tube and shaken, then placed in a centrifuge. This process allows the less dense "light" minerals to float to the top and the more dense "heavy" minerals, including apatite, to settle at the bottom of the test tube. The lower portion of the test tube is frozen with liquid nitrogen and the light minerals are removed from the tube. The heavy minerals are rinsed and move on to magnetic separation. By using a magnet, the metallic minerals are

removed from the samples. At this point, the samples have been reduced to include apatite, zircon, and other non-metallic minerals of similar density. Next, the samples are analyzed under the microscope for apatite/zircon picking.

3.4. Mineral Picking

With the aid of a microscope, euhedral apatite grains are selected from the samples. The apatite mineral is transparent to translucent, usually green or colorless with a hexagonal bipyramidal crystal system. An average of ten apatite grains of similar size was collected from each sample. These apatite grain selections were based on obvious facets and terminations, and an absence of inclusions and zoning. Similar-sized minerals provide more or less consistent measurements of isotopic concentrations. By selecting euhedral apatite grains, it is ensured that each mineral is, in fact, an original and not a fragment of a larger grain that has been broken. A lack of inclusions is required for accurate isotope measurement. Any stray mineral inclusion could hold some amount of U, Th, or He, thus throwing off their ratios and providing a misleading geologic age. Also, any inclusions, impurities, or fractures may provide an additional pathway for diffusion of ^{4}He, thus negating predicted closed-system behavior of the apatite grain after reaching closure temperature.

3.5. Apatite (U-Th)/He Thermochronologic Dating

(U-Th)/He measurements and Fission Track (FT) corrections were conducted at Arizona State University. He ages were calculated and represented statistically and graphically. Thermal models were made with HeFTy software with RDAAM calibration.

3.5.1. Overview

Low-temperature Apatite (U-Th)/He thermochronologic dating, also known as Apatite Helium (AHe) dating, can be used to understand the cooling history at relatively shallow depths of less than 5 km (Figure 3.4.) as compared to other thermochronometers (Table 3.1). Concentration levels of He-4 (^{4}He) accumulation due to the radioactive decay (figure 3.5) of unstable isotopes Uranium-238 (^{238}U), Uranium-235 (^{235}U), Thorium-232 (^{232}Th), and Samarium-147 (^{147}Sm) (Reiners et al., 2005) in apatite grains are extracted from minerals in rock samples. This is the lowest temperature

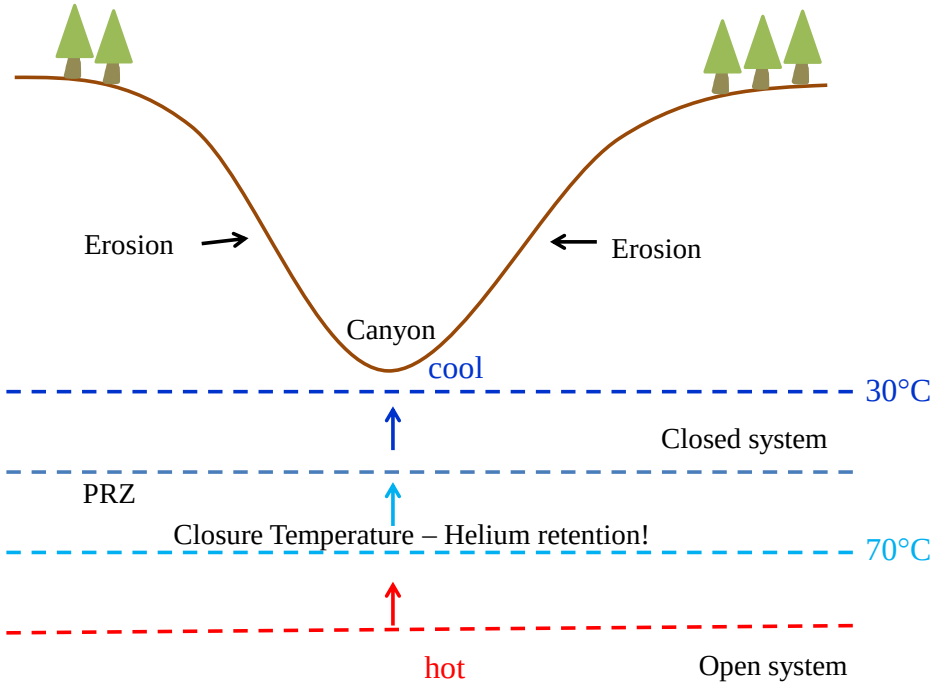

Figure 3.4: Canyon incision model. This conceptual profile of canyon incision illustrates He retention, and temperature conditions in closed and open systems. The Partial Retention Zone (PRZ) represents the temperature range within which He can be either retained or diffused from apatite grains.

Source: Created by author.

thermochronometer, and is important because it can document the thermal history at temperatures between 70°-30°C (Table 3.1) in the uppermost part of the crust. This temperature range is known as the Partial Retention Zone (PRZ). At temperatures within the PRZ (Figure 3.4), apatite crystals can both retain and diffuse He produced by radioactive decay (Wolf et al., 1998; Ehlers and Farley, 2003; Fitzgerald et al., 2006; Reiners and Brandon, 2006; Shuster et al., 2006;).

Radioactive Decay System	Mineral	Closure Temperature (°C)
U-Pb	zircon	>900
	titanite	550-650
	monazite	~700
	apatite	425-500
$^{40}Ar/^{39}Ar$	Hornblende	400-600
	Biotite	350-400
	Muscovite	300-350
	K-feldspar	150-350
Fission-track	Titanite	240-420
	Zircon	230-350
	Apatite	90-120
(U-Th)/He	Titanite	160-220
	Zircon	160-200
	Apatite	30-70

Table 3.1. Thermochronometer closure temperatures. (U-Th)/He apatite is a low-temperature thermochronometer with a closure temperature of 30°-70° C (Reiners, 2005).

In apatite (U-Th)/He Thermochronology, daughter product ^{4}He particles are retained within apatite mineral as the apatite passes through the closure temperature of approximately 68°C. These ^{4}He particles (Figure 3.5) result from the radioactive decay of ^{238}U (Farley, 2000).

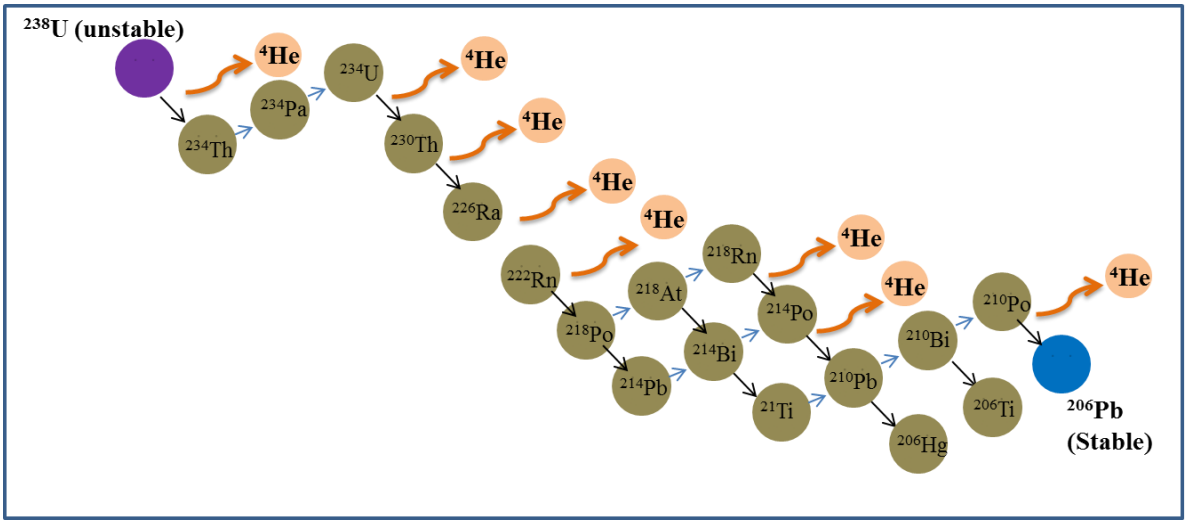

Figure 3.5: ^{238}Udecay chain. The radioactive decay chain of ^{238}U to ^{206}Pb produces eight ^{4}He daughters (Rosholt, 1959).

AHe dating can be applied at a depth of roughly 1-3 km, considering the average geothermal gradient is around 25°C/km (Reiners et al., 2005). As the parent isotopes in apatite decay over time, ^{4}He accumulates within the mineral, while diffusing at a rate that is dependent on the temperature and He diffusivity of the mineral (Reiners et al., 2005). Extraction of (U-Th)/He data and application of thermal modeling produce the best possible thermal history of a region. (U-Th)/He concentration data input to the HeFTy software produces time-temperature models of the likely thermal history for each apatite

grain. The time-temperature curves in the thermal model represent the most likely routes taken from deep burial to the surface, or periods of time spent at various temperature levels associated with the geothermal gradient and other geologic constraints.

3.5.2. Factors for Consideration

A thermochronologic system cannot be assumed to exhibit an abrupt change from open to closed system behavior (Figure 3.4) at the point closure temperature is reached (Reiners et al., 2005). A closed system signifies no interaction with material outside the apatite grain. An open system allows interaction between the material inside and outside the grain. There are variations in this process depending on temperature, grain size, zonation, radiation damage, and fission track length (Figure 3.6). The conditions experienced by each apatite grain, its dimensions, and quality affect diffusion behavior over its journey through the geothermal gradient. Other issues include alpha ejection within 20 μm (micrometer) of the crystal boundaries (Figure 3.6i). The alpha particle emission causes fission tracks in the apatite grains, which can provide avenues for increased He diffusion out of the crystal. High fission track density in apatite crystals denotes enhanced He diffusion. Each fission track provides an avenue of He migration out of the grain. This radiation damage can cause issues in the age calculation but is accounted for based on crystal dimensions with a FT correction. It can be adjusted for in the RDAAM (Radiation Damage Accumulation and Annealing Model in HeFTy software (Figure 3.6ii). In addition, bad neighbors or adjacent minerals can alter isotope concentrations (Figure 3.6iii). Diffusion kinetics can also be affected by zonation within apatite grains, or areas of independent crystal growth patterns (Figure 3.6iv). These zones can exhibit settings of altered diffusion factors. Zoning in apatite crystals can develop

from chemical imbalance during crystal growth (Reiners et al., 2005). Inclusions, or mineral crystals inside other mineral crystals, can alter the isotopic concentration measurements performed in thermochronology by adding their own isotope concentration to the larger crystal, or the apatite crystal in this case (Figure 3.6v).

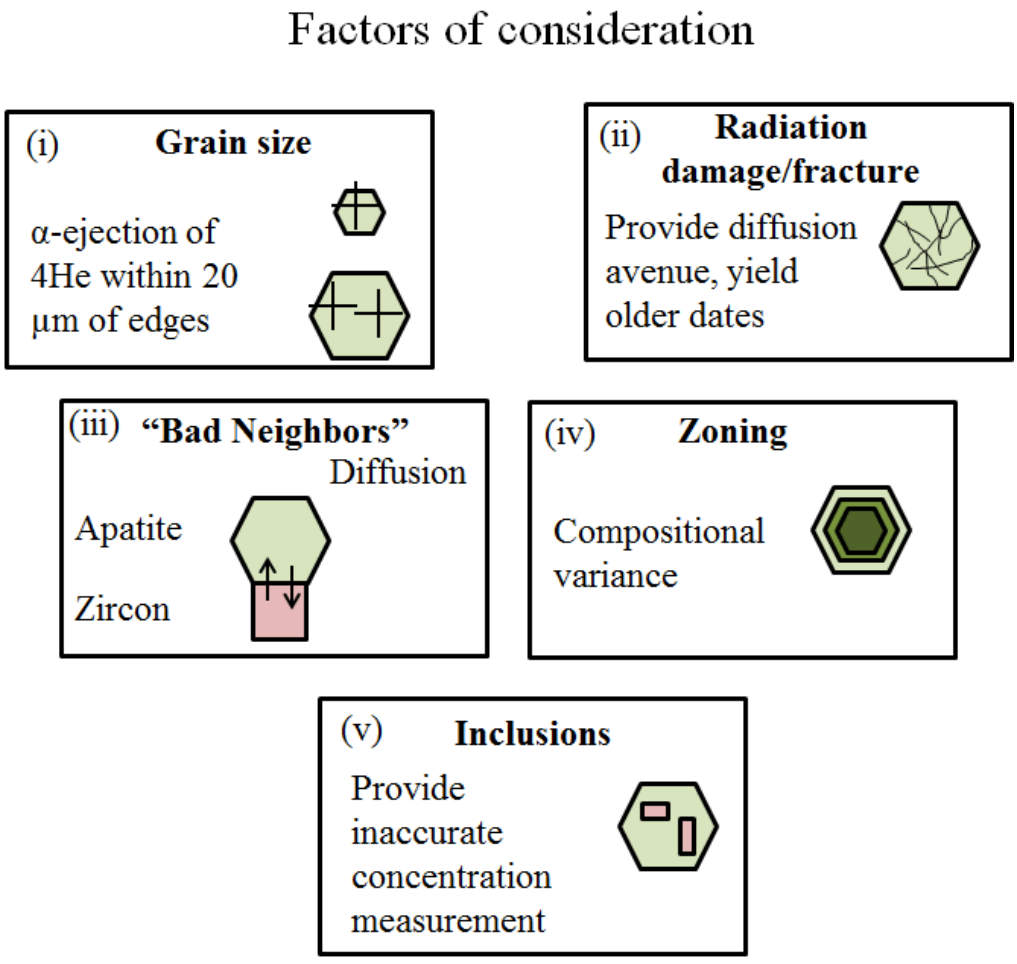

Figure 3.6: Factors of consideration. Common factors that can influence AHe dates include grain size, bad neighbors, zonation, inclusions, radiation damage, and fission track length in apatite grains.

3.5.3. Apatite Selection and Documentation

Selecting euhedral grains ensures that each grain is, in fact, an original grain and not a fragment of a larger grain that has been broken. A lack of inclusions is required for accurate isotope concentration measurement. Any stray mineral inclusion could hold some amount of U, Th, or He, thus throwing off their ratios and providing a misleading geologic age. Any inclusions, impurities, or fractures may provide additional pathways for diffusion of ^{4}He, thus negating predicted closed-system behavior of the apatite grains after reaching closure temperature. Finally, a total of 49 euhedral apatite grains were selected from the samples, with radii ranging from 32.9 to 126.7 µm. Figure 3.7 shows examples of a few euhedral single apatite grains that were used in this study.

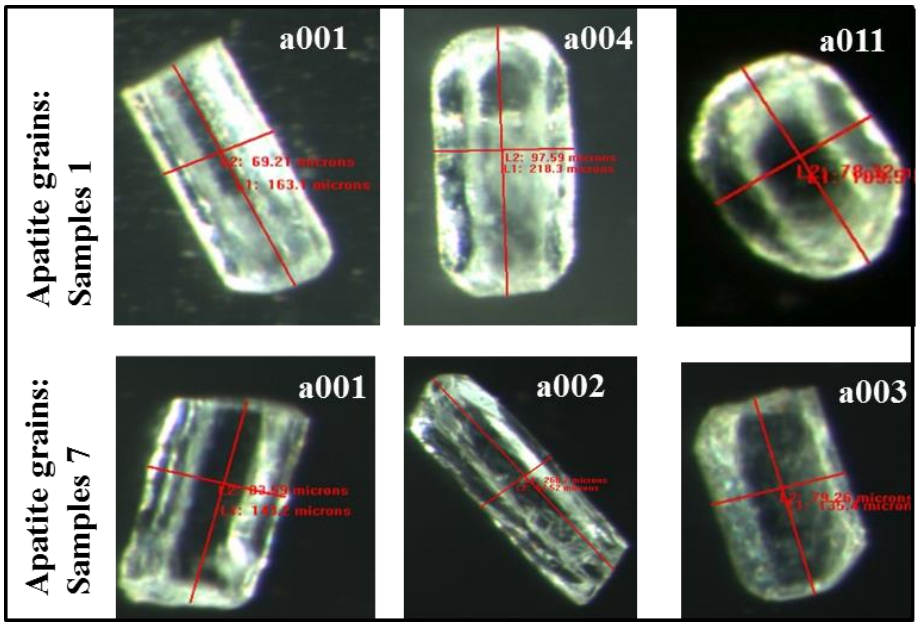

Figure 3.7: Apatite grain images. Shown are example images of apatite grains that were dated in this study. Note the apatite grains in the first row are from sample 1 and apatite grains from the second row are from sample 7. Source: Photos by Matthijs van Soest.

3.5.4. U, Th, and He Measurement

U, Th, and He concentrations of individual apatite grains were measured using the ASI Alphachron and ICP-MS at the Group 18 Laboratories at Arizona State University. Individual apatite grains in foil packets were placed in the ICP-MS to measure Uranium and Throrium concentrations. The samples were also heated with a laser to measure the He in the ASI-Alphachron.

3.5.5. Age Calculation

Following U, Th, and He concentration acquisition, the data were inserted into the following formula to calculate the AHe age (e = base of natural logarithm, t = age (Ma): $^{4}He \cdot 8^{238}U(e \cdot {}^{8}t \cdot 1) \cdot 7^{235}U(e \cdot {}^{7}t \cdot 1) \cdot 6^{232}Th(e \cdot {}^{2}t \cdot 1) \cdot {}^{147}Sm(e \cdot {}^{147}t \cdot 1)$.

The Relative Standard Error (RSE) is 3% to 5% for AHe ages (Reiners and Brandon, 2006). These are calculated based on error throughout the heating/degassing for He, U, and Th measurement processes.

3.5.6. Alpha Ejection Correction

Alpha ejection (Fission Track) correction (Figure 3.8) is a technique used to adjust raw AHe ages closer to their actual ages. The alpha particle emission causes fission tracks in the apatite grains, which can provide avenues for increased He diffusion. This practice is based on the assumption of increased alpha particle ejection within 20 μm of the crystal boundaries. Corrections are typically less than 5-10% and are determined by the crystal dimensions.

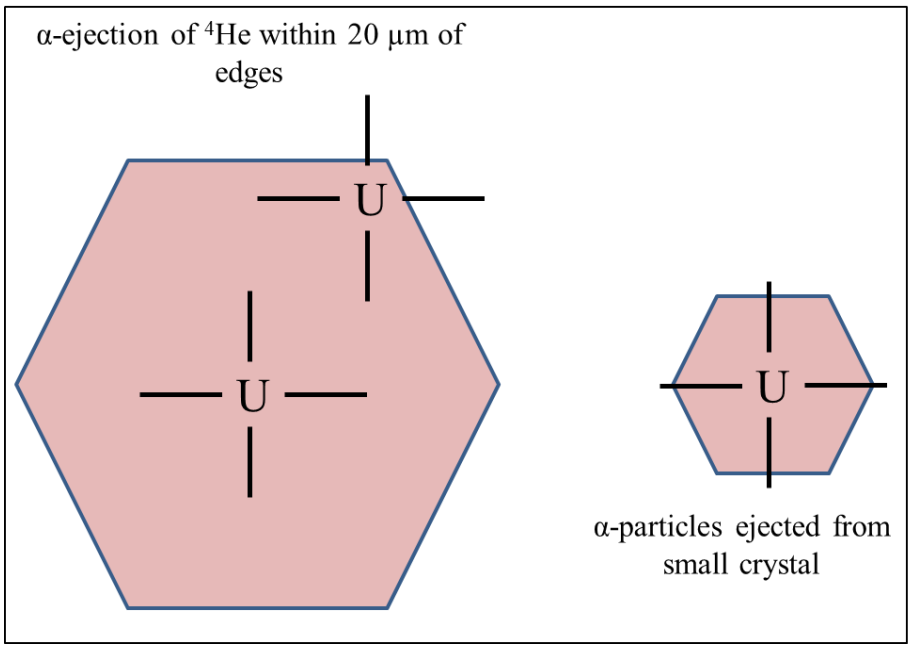

Figure 3.8: Alpha Ejection Correction. Fission Track (FT) Correction accounts for loss of He from radiogenic decay of Uranium within 20 µm from edges of each apatite crystal.

3.5.7 Statistical and Graphical Representation of AHe Age Data

Several graphical and statistical techniques were used in an effort to uncover patterns and find interpretations of the (U-Th)/He data. Chauvenet's Criterion for Outlier Exclusion was performed to narrow the ages to a more appropriate range. The ages were analyzed based on their size and location, and interpreted to explain the reason for age dispersion and any patterns found. To interpret the cooling ages/history, outlier exclusion was employed to exclude outlying grains from AHe age data based on their distance from the mean of each sample. This distance is a multiple of the standard deviation determined by the number of grains in each sample (Fitzgerald et al., 2006; Long and Rippeteau, 1974).

AHe age was graphed versus elevation in the sample profile to observe any correlations. This technique includes estimation of the actual AHe age between the mean

and minimum age for each sample, and observation of any pattern in actual age versus grain radius. This practice allows examination of any patterns/correlations between samples to determine possible thermal history. Minimum AHe age versus mean AHe age was graphed to compare minimum age and weighted mean age for each sample (Fitzgerald et al., 2006). AHe Age (Ma) versus grain radius (μm) was graphed to compare age versus radius relationships. This technique can identify relative cooling rate between the samples. This is a standard statistical technique (Fitzgerald et al., 2006; Long and Rippeteau, 1974) to exclude obvious outliers from a set of numbers based on their distance from the mean value lying within a multiple of the standard deviation.

3.5.8. Thermal Modeling

Thermal modeling was performed using the HeFTy program (Ketcham, 2005). The HeFTy software, allows both forward and inverse modeling. Forward modeling is used to view how thermochronometers behave under varying time-temperature conditions. Time and temperature information is entered into the software (Figure 3.9), and the product is thermochronologic information: i.e., He diffusional profiles. This is a useful feature as it is a quick way to view the effects of variations in time and temperature on the diffusion properties of chosen specimens. Monte Carlo Inverse Modeling, which is used in this study, entails the opposite of forward modeling. In this model, when thermochronologic and geologic information are added, then HeFTy searches time-temperature paths and provides "acceptable," "good," and "best fit" curves for time-temperature history. These inputs include parts per million of radiogenic isotope concentrations (U, Th, and He), measured age, radius of grain, and known geological constraints of known time-temperature limitations.

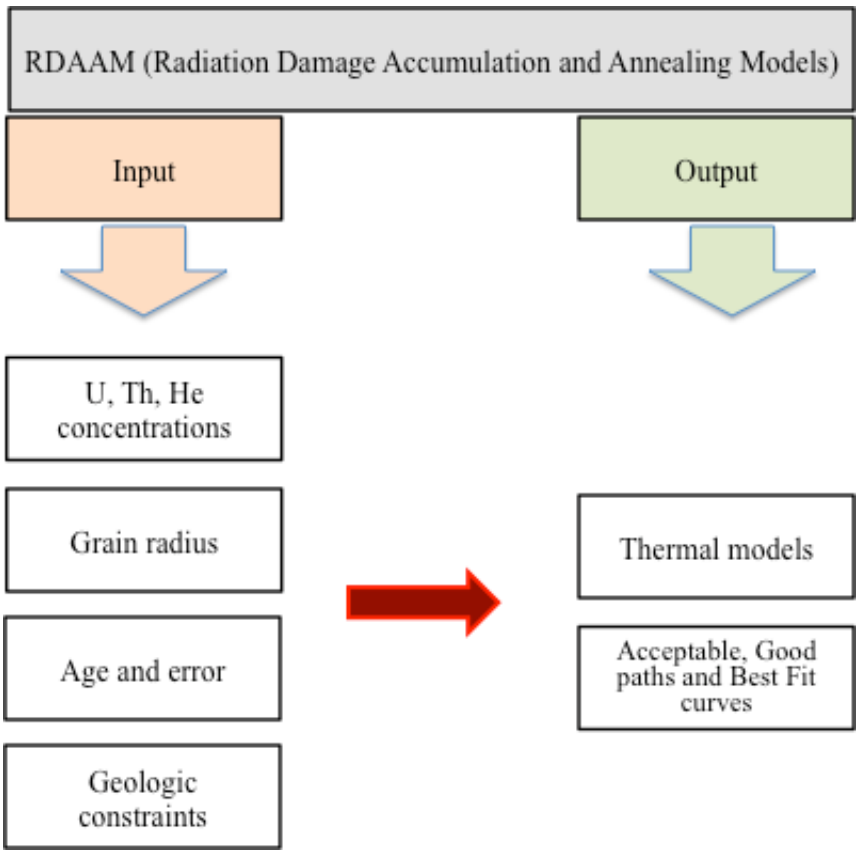

Figure 3.9: Thermal Modeling flow chart. The flow chart displays input and output for inverse thermal model in HeFTy program.

The Radiation Damage Accumulation and Annealing (RDAAM) model (Flowers, et al., 2009) calibration provided statistically reasonable time-temperature paths for the apatite grains. The RDAAM incorporates fission track density as a factor of (U-Th)/He age calculation based on its influence on He diffusion kinetics in apatite grains. Due to the complex geologic history of the region, the RDAAM provides suitable parameters for analysis of this apatite suite, which has been subjected to conditions prone to partial resetting as a result of the deposition of the overlying 1 km-thick flood basalt at 30 Ma and ensuing temperature increase. Following thermal modeling, the cooling rate was inferred based on the "best fit curve" for the time-temperature history.

CHAPTER 4: RESULTS AND INTERPRETATION

Apatite (U-Th)/He thermochronology was carried out to constrain the thermal/cooling history of the study area resulting from plateau unroofing. Single grain apatite (U–Th)/He cooling ages (AHe) were obtained from six Neoproterozoic basement rock and two Mesozoic sedimentary rock samples collected from a vertical profile along the Blue Nile Canyon on the Ethiopian Plateau (Figures 3.2 and 3.3). This chapter explains the results from the number of statistical approaches and thermal modeling explained in Chapter 3. First, an interpretation is made from the statistical methods, which plot the dates with grain morphology (e.g., radius, length, volume), U, Th, He concentration, F_T factor) to explore any pattern or correlation (Table 4.2). Next, inverse thermal models using these dates are interpreted for constraining thermal/cooling history related to the geologic history of the study area.

The (U-Th)/He ages of the apatite grains range between 64 to 460 Ma (Figure 4.1). This wide range of AHe ages in single grains does not define a simple age-elevation relationship, as the ages are much older than those reported from similar elevations by Pik et al. (2003) from a nearby locality. These data also show intra-sample AHe age variation (e.g., sample 1 shows age ranges that varies from 64.1 Ma to 179.6 Ma; sample 2 shows age variation from 71.7 Ma to 120.8 Ma; Figure 4.1). Thus, caution should be used when interpreting these single grain AHe ages.

Table 4.1: Summary of statistical methods and patterns.

Statistical/Graphical methods	Pattern
(U-Th)/He age v. Radius (grain size)	Weak correlation except one sample
(U-Th)/He vs. F_T correction	Weak or no correlation except one sample
(U-Th)/He age vs. U, Th and Th/U	Weak to no correlation
Radius vs. F_T Correction	Positive correlation with an R^2 value of 0.995
Length/Radius vs. Radius	Weak to no correlation
Fission Track correction vs. Volume	Positive correlation with an R^2 value of 0.992
Minimum Age and Mean Age vs. Elevation	Slow and rapid cooling
(U-Th)/He age vs. Frequency	Unimodal distribution with peak at cluster of 75-100 Ma
Effective Uranium (eU) vs. (U-Th)/He age and radius vs. eU	Positive correlation; Weak positive correlation

4.1. Grain Morphology and Selection

A number of possible factors can be involved for this AHe age variation, which includes grain size or radius, inclusions, fracture, etc., as discussed in section 3.5.2. In this study, all the grains were carefully selected for (U-Th)/He dating based on euhedral shape, absence of obvious inclusions and fractures, and transparency of each grain carefully inspected under crossed polars of the petrographic microscope (Table 4.1). The majority of the dated apatite grains are euhedral shaped without any obvious inclusions. Only a few grains showed some spots that might be micro-inclusions, which were not observed during optical inspection. These micro-inclusions may add excess ^4He (Lippolt et al., 1994) to these grains that may lead to old/anomalous ages for some of these grains (e.g., 460 Ma apatite grain a2 in sample 8).

4.2. (U-Th)/He Age vs. Radius (grain size)

Grain size or radius of the apatite grains analyzed in this study varies from 32.9 to 98.3 µm, and the F_T correction factor ranges from 0.594 to 0.851. The plot of (U-Th)/He age

vs. radius (Figure 4.2) shows variation of single grain cooling age with grain size for all the samples collected along the vertical profile of the Blue Nile Canyon. By plotting the AHe age versus the radius of each apatite grain per sample, age dispersion is observed. Samples with greater age range in single grain AHe ages suggest that these samples cooled relatively slowly or had an extended residence in the He partial retention zone (PRZ). For example, sample 1 (32.9-56.9 μm), 2 (34.7-98.3 μm), 3 (34.4-93.4 μm), 5 (36.1-54.7 μm) and 7 (36-42.6 μm) have R^2 values of 0.043, 0.002, 0.019, 0.089 and 0.007 respectively. These samples may have had longer residence in the PRZ and higher closure temperatures. In this case, U and Th distributions are likely to be non-homogenous with long PRZ residence time (Fitzgerald et al., 2006). Sample 6 has R^2 values of 0.561, which may indicate short residence time in the PRZ. Sample 8 was not interpreted because of the limited number of only two apatite grains found in the sample. Samples 1 and 5 show the greatest single variation in their single grain age, which can suggest slow cooling (e.g., Reiners and Farley, 2001) Thus, samples with small variation of grain size with single grain AHe age likely underwent rapid cooling.

Larger grains will likely yield older AHe age (the older the age, the higher the eU concentration) if the dispersion is for grain size variation (Fitzgerald et al., 2006; Flowers et al., 2009). Thus, the distribution of grain size may be a controlling factor of the single grain age variation but not the dominant factor for the dated grains. However, calculating sample cooling rates, which is not the scope of this study, may provide valuable information on the age dispersion. F_T correction factor (which has been applied to single grains for α-particle ejection) may also play a role in increasing the age variation with different U and Th concentrations. Forward thermal modeling, which is discussed at the

end of this chapter, was used as well to decipher if the grain size was a cause for intra-grain age variation.

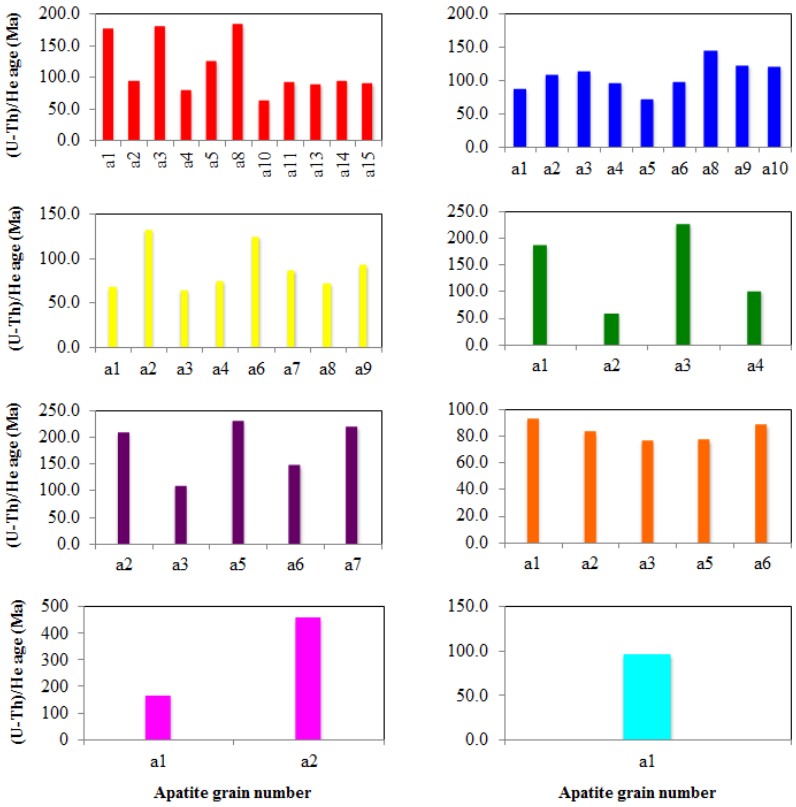

Figure 4.1: Grain Morphology and Selection. Single (U-Th)/He ages for each apatite grain in each of eight samples, one through nine, from left to right and descending. The x-axis displays the apatite grain number, and the y-axis is age (Ma).

Apatite (U-Th)/He dates	Apatite grain morphology
Sample 1 (all grains)	Euhedral, no obvious inclusion under crossed polars, transparent, two grain has some spots that could be inclusion 63-250μm
Sample 2 (all grains)	Euhedral, transparent, no obvious inclusion under crossed polars, 63-250μm
Sample 3 (all grains)	Euhedral, transparent, no obvious inclusion under crossed polars, 63-250 μm
Sample 5 (all grains)	Euhedral, transparent, no obvious inclusion under crossed polars. One grain has some spots that could be inclusion, 63-250 μm
Sample 6 (all grains)	Euhedral, transparent, no obvious inclusion under crossed polars, two grain has some spots that could be inclusion, 63-250 μm
Sample 7 (all grains)	Euhedral, few semi-euhedral, transparent, no obvious inclusion under crossed polars, 63-250 μm
Sample 8 (all grains)	Rounded euhedral, transparent, no obvious inclusion under crossed polars, 63-250 μm
Sample 9 (all grains)	Euhedral, transparent, no obvious inclusion under crossed polar, 63-250 μm

Table 4.2: Apatite grain morphology. Included is a morphologic description of the apatite grains in each sample from the Blue Nile Canyon.

4.3. (U-Th)/He age vs. Fission Track (F_T) Correction

The F_T correction factor can also increase the age variation when applied to grains with different U, Th distribution (Farley et al., 1996). F_T correction, a geometric correction, was performed for each grain based on the grain geometry (euhedral shape) and grain size (specifically, surface area to volume ratio) to correct for the α-particle or ^{4}He ejection from each grain during α-particle decay events (Farley et al., 1996). In the plot of (U-Th)/He age with F_T correction, the R^2 value for each sample indicates weak to no correlation except sample 6, which has an R^2 value of 0.570. Crystal dimensions are not suspected to be responsible for AHe age dispersion (Figure 4.3). In this study the FT correction factor varies from 0.594 to 0.851 with an average 8% of 2σ standard deviation for all the grains of 63-250 μm width, suggesting that most of the ^{4}He or α-particle retention is in these apatite grains.

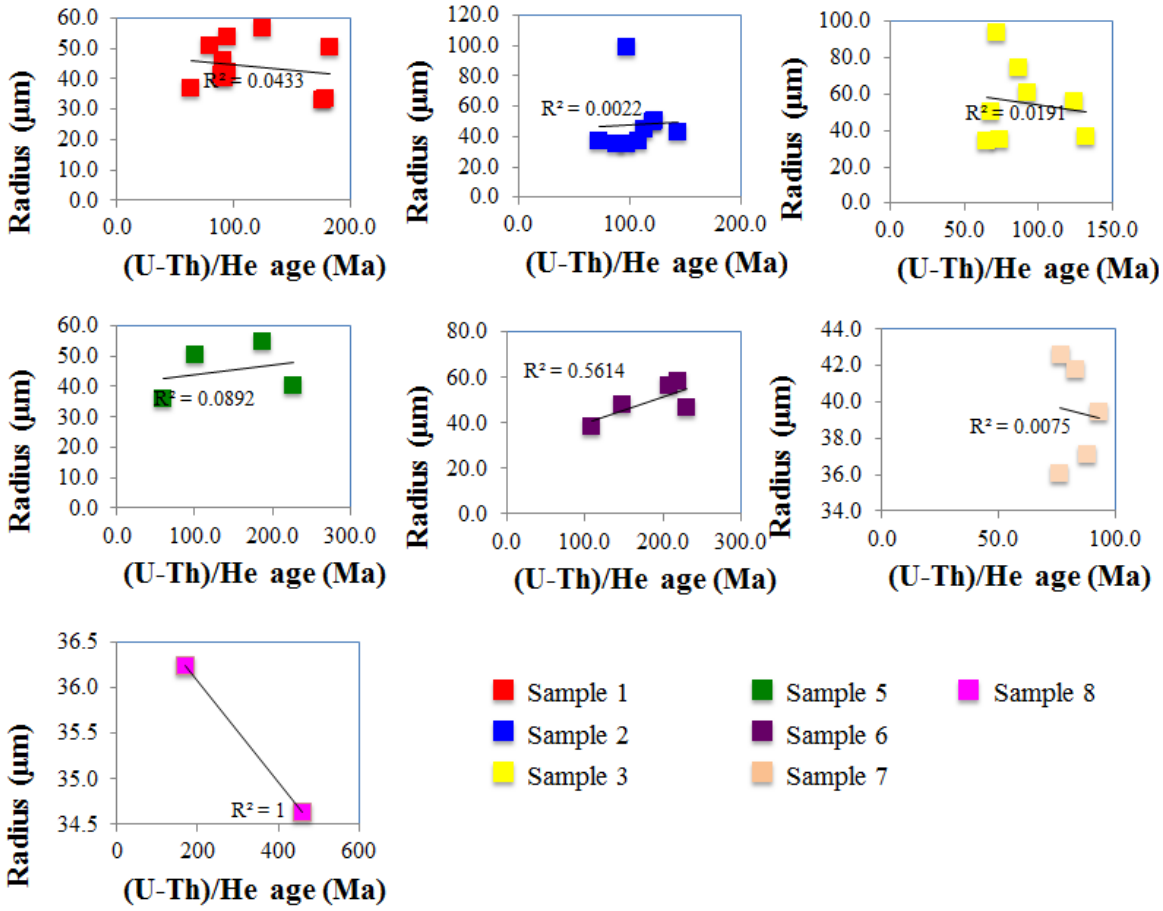

Figure 4.2: (U-Th)/He Age vs. Radius (grain size). Displayed are plots of apatite (U-Th)/He dates against radii for each sample.

4.4. (U-Th)/He age vs. U, Th and Th/U Concentration

The R^2 value for (U-Th)/He age versus uranium concentration is 0.009. This uranium concentration is not responsible for AHe age dispersion (Figure 4.4i). The R^2 value for age versus thorium is 0.0114. This implies no correlation (Figure 4.4ii). Th concentration is not responsible for AHe age dispersion. The R^2 value for Age versus Thorium/Uranium is 0.0249. This implies no correlation and that thorium/uranium concentration are not responsible for AHe age dispersion (Figure 4.4iii).

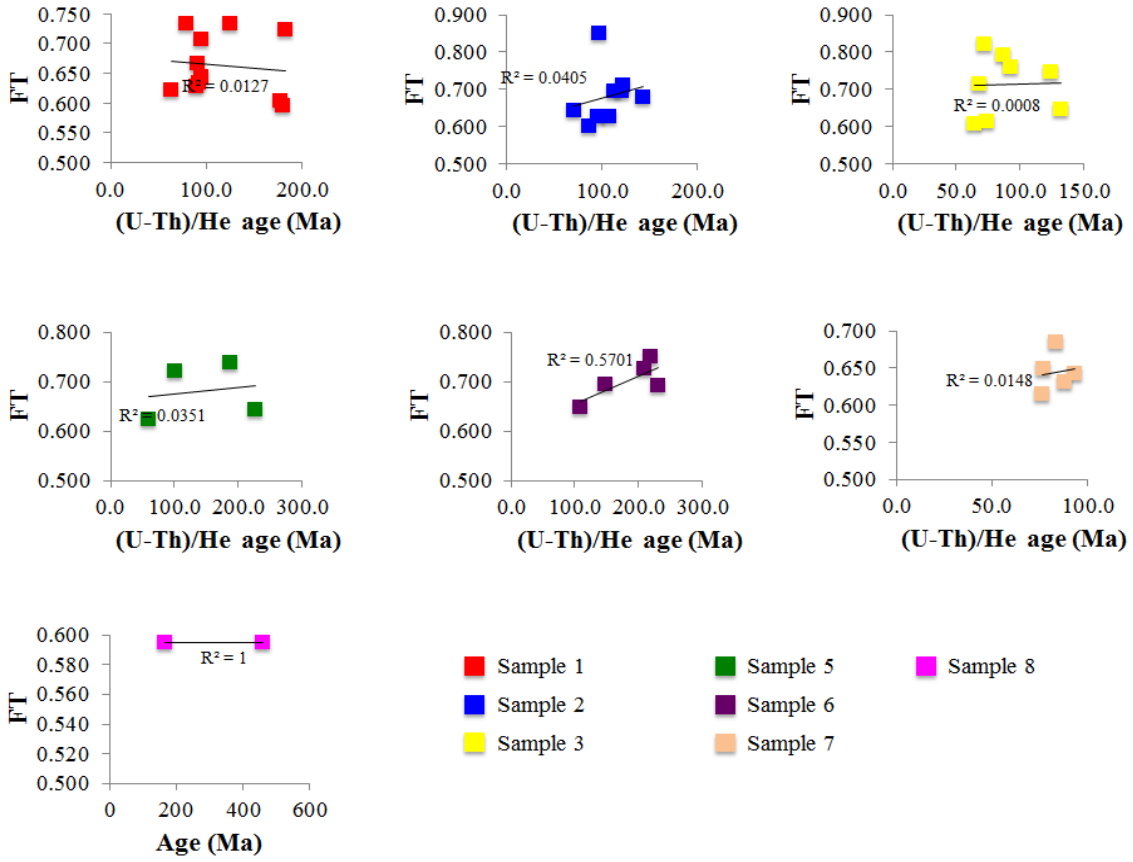

Figure 4.3: (U-Th)/He age vs. Fission Track (FT) Correction. Displayed is plot of AHe age and radius in apatite grains for each sample.

4.5. Radius vs. F_T Correction

The radius of each dated grain was plotted as a function of F_T correction, which shows positive correlation with an R^2 value of 0.995 (Figure 4.5). F_T correction value is calculated from the dimensions of each apatite crystal, including radius. Therefore, a high R-squared value is to be expected since F_T correction is derived from crystal dimension measurements. From an experimental study, Farley et al. (1996) concluded that about 64% of ^{4}He decays from ^{238}U and 58% of ^{4}He decays from ^{235}U in apatite grain with 40 μm radius. In order to minimize the source of ^{4}He uncertainty, this study calculated the mean F_T.

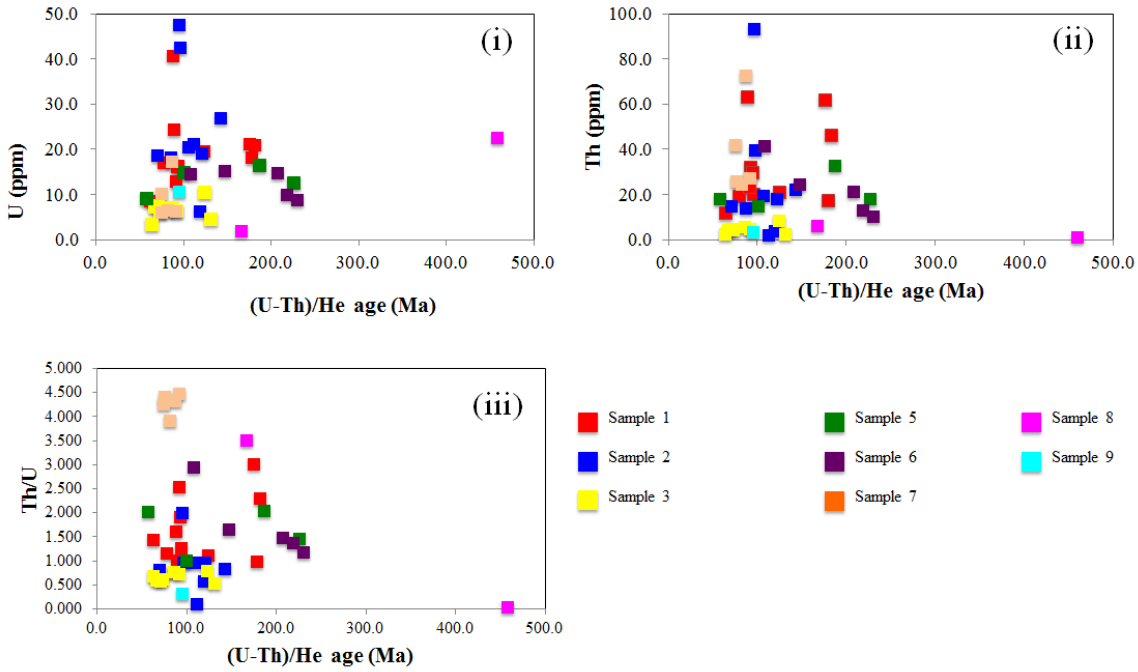

Figure 4.4: (U-Th)/He age vs. U, Th and Th/U Concentration: (i) Plot of AHe age and U concentration of apatite grains for each sample; (ii) Plot of AHe age and Th concentration of apatite grains for each sample. (iii) Plot of AHe age and Th/U of apatite grains for each sample.

The apatite grains have radii between 32.9-98.3 μm. Seventeen grains have radii between 32.9-39.5 μm, 13 grains have radii between 40.3-49.3 μm, 11 grains have radii between 50.1-58.1 μm, one grain has a radius of 60.9 μm, one grain has a radius of 74.3 μm, and two grains have radii of 93.4 and 98.3 μm, respectively. Most of the grain radii are within 60 μm, indicating 4He retention rather than diffusion from the grains.

4.6. Length/Radius vs. Radius

The Length/Radius versus Radius graph provides a weak or no correlation. Crystal growth along the Y- and Z-axes progresses more quickly than the X-axis, and the grains of this suite exhibit no prevailing dimension pattern (Figure 4.6).

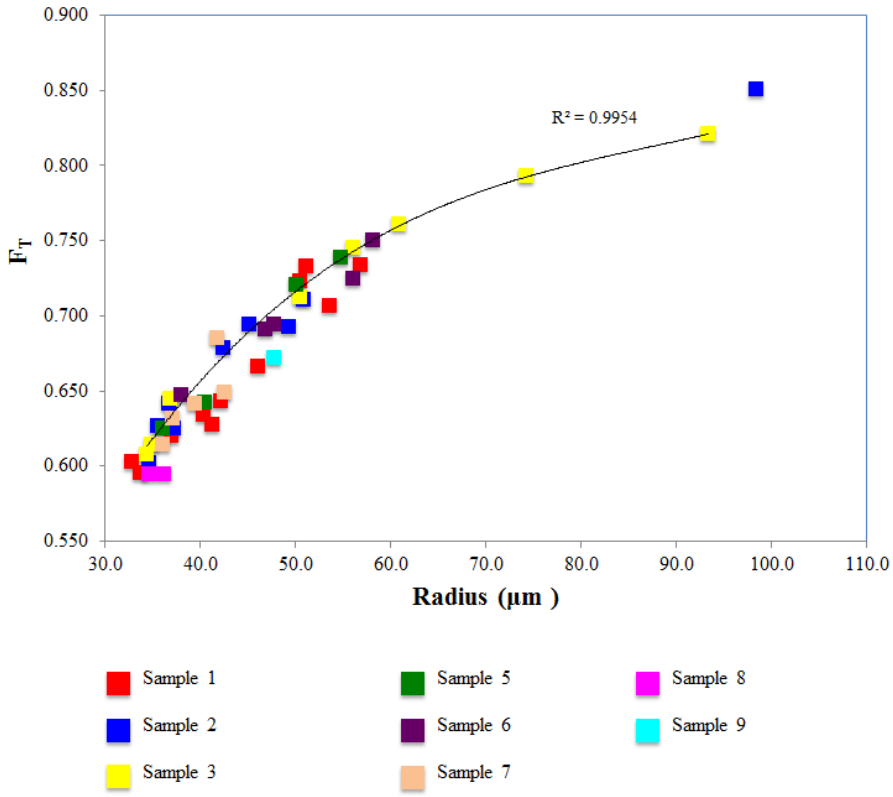

Figure 4.5: Radius vs. F_T Correction. Exponential trend between F_T correction and radius of apatite grains for each sample.

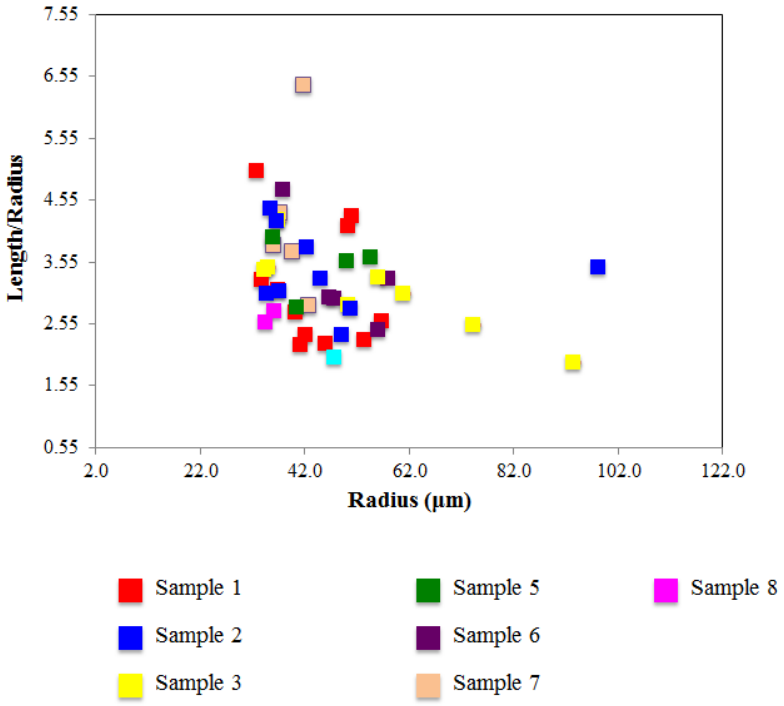

Figure 4.6: Length/Radius vs. Radius. Positive correlation between length/radius vs. radius of apatite grains for each sample.

4.7. Fission Track correction vs. Volume

The exponential trend of fission track (F_T) correction versus volume has an R^2 value of 0.992 (Figure 4.7). Exponential trend is expected as the F_T correction value is calculated to correct the age based on the dimensions of each apatite grain, and volume is derived from the same dimensions. The significance of this strong correlation is that the F_T correction technique is supported by the trend.

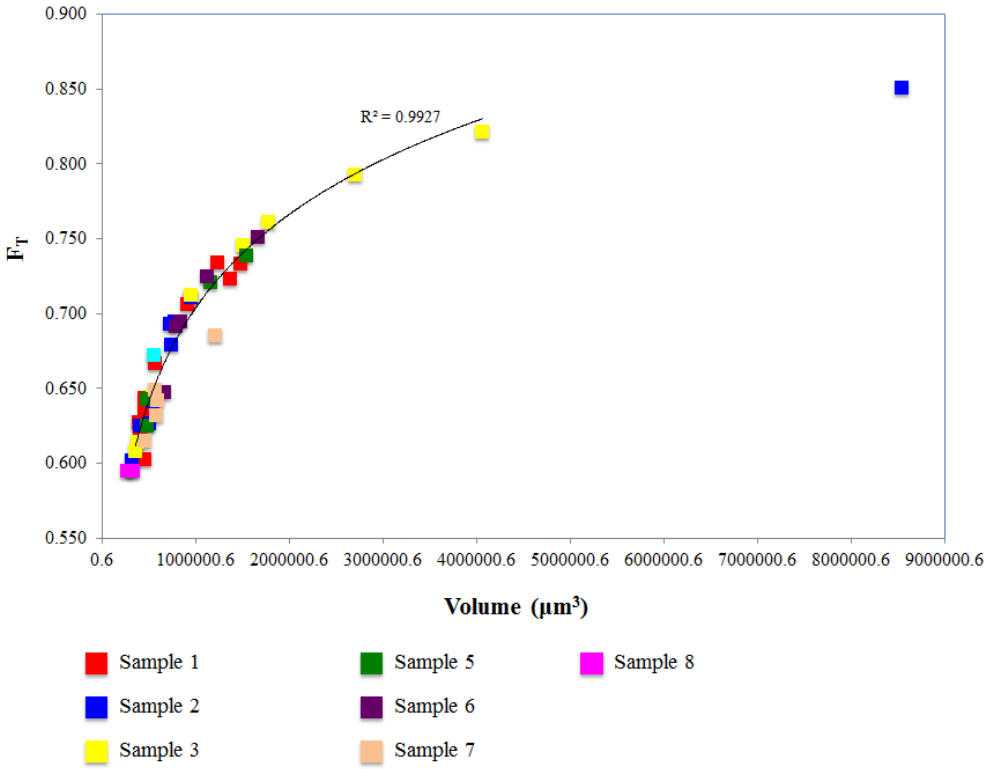

Figure 4.7: Fission Track correction vs. volume. Exponential trend is displayed between F_T correction and volume of apatite grains for each sample.

4.8. Minimum Age and Mean Age vs. Elevation

For single grains with considerable AHe age dispersion, a weighted mean age (Figure 4.8) was calculated to predict actual age. The actual AHe age is interpreted to be between the Minimum and Mean ages. Samples 1, 2, and 3 display a decrease in AHe age with increasing depth. Samples 3, 5, 6, and 8 display an increase in AHe age with increasing depth, while samples 7 and 9 fall between these two conditions. The increase of AHe age with depth is expected in a canyon incision. The older ages and large age ranges shown in the plot likely suggest slow cooling followed by rapid cooling.

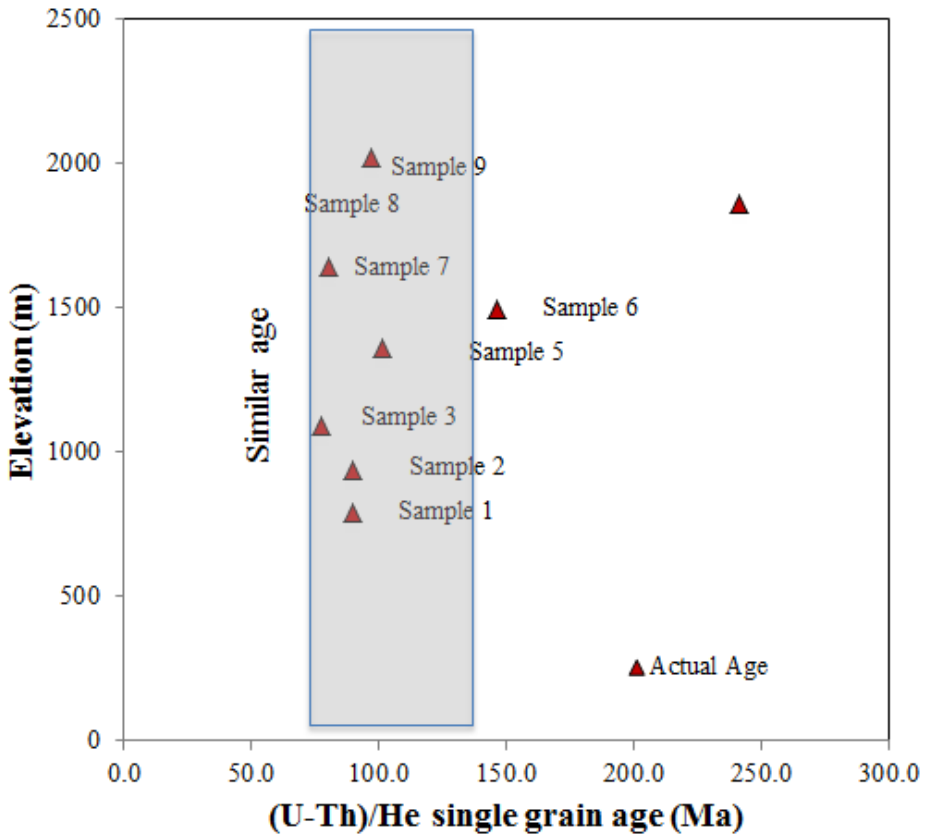

Figure 4.8: (U-Th)/He Age vs. Elevation. Ages were calculated as a mean of minimum and mean ages.

4.9. (U-Th)/He age vs. Frequency

AHe ages for all samples were classified in 25 Ma increments to observe frequency of age clusters, with all samples ranging from 0-250 Ma. The results show a possible unimodal distribution with peaks at 75-100 Ma (Figure 4.9). This could suggest two age clusters of 75-100 Ma and 150-175 Ma but, based on the limited sample ages within 150-175Ma, it is interpreted as part of this unimodal distribution. Perhaps since the major cluster is around 75-100 Ma, it may be interpreted that the actual age of the apatite suite lies near 75-100 Ma. Further, sample 7 (the sample with least dispersion) consists of 5 grains, which have AHe ages from 76-93 Ma.

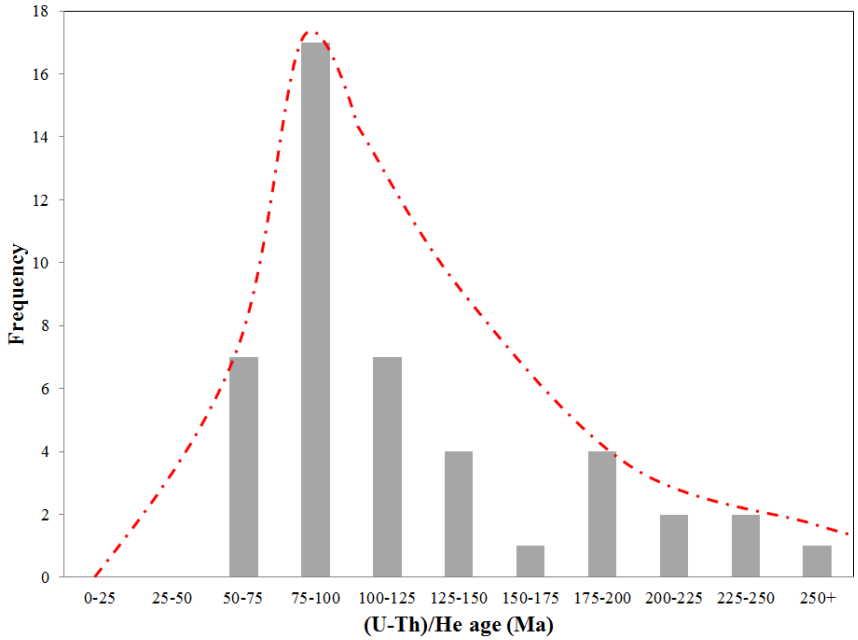

Figure 4.9: (U-Th)/He age vs. Frequency. Plot of the frequency of apatite (U-Th)/He dates for all samples at 25 Ma increment. This plot shows most of the dates are clustered between 75-100 Ma age ranges.

4.10. Effective Uranium (eU) vs. (U-Th)/He age

The (U-Th)/He ages have effective uranium (eU) concentrations ranging from 3 to 69.6 ppm. The R^2 value for eU versus AHe Age for all samples is 0.192. This implies a weak correlation (Figure 4.10i). However, when eU values are plotted against (U-Th)/He ages for each sample separately, correlation exists in each of these samples (Figures 4.10ii to 4.10vi). These single grain ages show a distinct positive correlation with eU (Flowers et al., 2007).

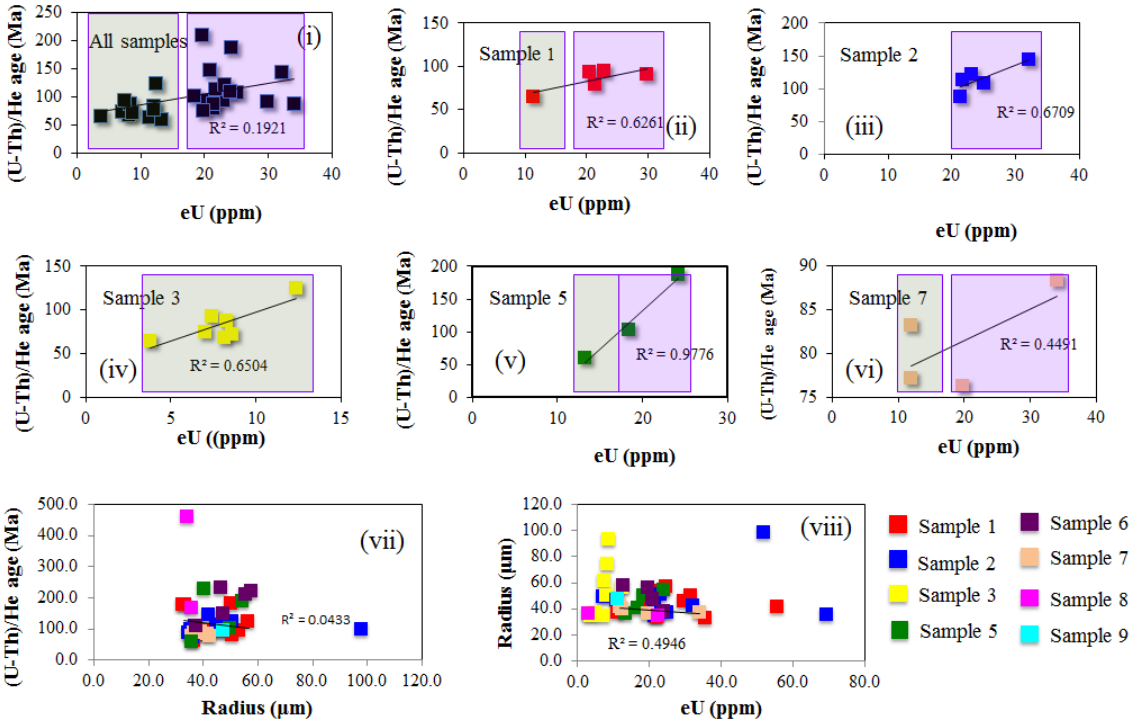

Figure 4.10: Effective Uranium (eU) vs. (U-Th)/He age. Displayed are plots of AHe age and eU concentrations in apatite grains from each sample. Purple and grey rectangles indicate high and low eU values respectively.

Apatite grains with higher eU will accumulate more radiation damage, and hence may retain more ^{4}He rather than diffusing it from grains (Shuster et al., 2006; Flowers et al., 2007; Flowers et al., 2009; Shuster and Farley, 2009; Ault et al., 2009; Flowers and Kelley, 2011). For example, in samples 1, 2, 5 and 7, eU is high (>20 to >40 ppm) and therefore yielded older ages. On the other hand, samples 1, 3, 5 and 7 have a low eU (<20 ppm) and yielded younger ages. When grain size (i.e., radius) is plotted against (U-Th)/He ages, a weak positive correlation exists for all grains with higher eU values (Figure 4.10 vii).

4.11. Thermal Modeling

A number of inverse thermal models were produced using the Radiation Damage Accumulation and Annealing (RDAAM) Model (Flowers et al., 2009) in HeFTy software. RDAAM provides a suitable calibration for this apatite suite, which has extensive radiation damage accumulation and annealing during extended residence at high temperature. In each model, geologic constraints were used to bracket the thermal/cooling history of the study area. Geologic constraints were based on: (1) the Triassic/Jurassic sandstone deposition; (2) 30 Ma flood basalt accumulation; and (3) current surface position. Between 250 and 145 Ma, the Triassic/Jurassic sandstone (Gani et al., 2009) was deposited, implying the contact between Neoproterozoic basement and sandstone would have been at a surface position with a temperature around 0-40°C. The 30 Ma flood basalt yielded a depth increase of ~1 km, with a potential temperature increase of ~40°C. The present-day surface residence offers a temperature constraint of 0-36.5°C. Inverse thermal models are included for apatite grains in all samples (examples of sample 1 and sample 3 are shown in Figures 4.11 and 4.12). The input data for each model consist of the average of each AHe age, error, radius, uranium concentration, and thorium concentration of the apatite grains from each sample location. The focus of interpretation of these models is to decipher thermal/cooling history from 30 Ma to present and to find out if age dispersion or older age will provide older cooling history.

For example, each grain in sample 1 used for thermal modeling (Figure 4.11) exhibits a relatively slow, steady cooling trend from 30 Ma to 10 Ma. Around 10 Ma, a rapid increase in cooling rate ensues until 0 Ma. Sample 3 (Figure 4.12) shows a sharp increase in temperature at 30 Ma from ~50°C to 75°C, and then quickly cools to ~47°C

by 29 Ma. From 29 Ma to 8 Ma, it displays a steady, slow cooling with a faster cooling rate until 5 Ma, at which point it slows again until the present. Each of these thermal models varies in regards to its 30 Ma maximum temperature and cooling rates. However, each sample shows a general common trend of younger cooling history and rapid cooling sometime after 10 Ma. This late Neogene rapid cooling might be due to the incision of the Blue Nile likely linked to the Ethiopian Plateau uplift.

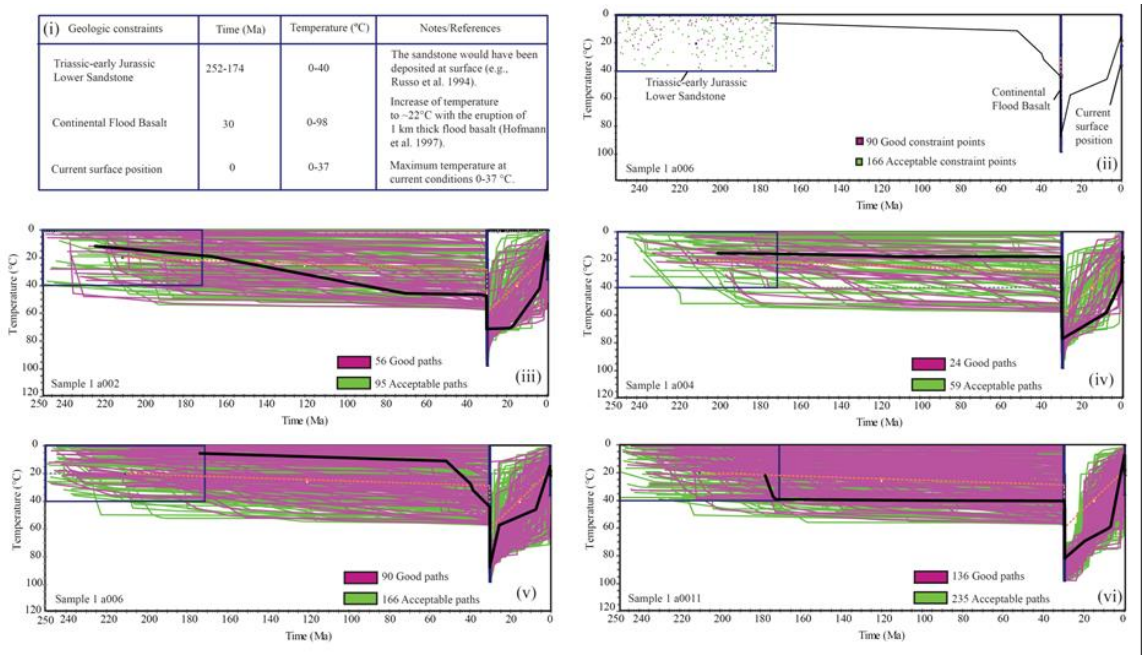

Figure 4.11: Thermal models of different apatite grains in sample 1.

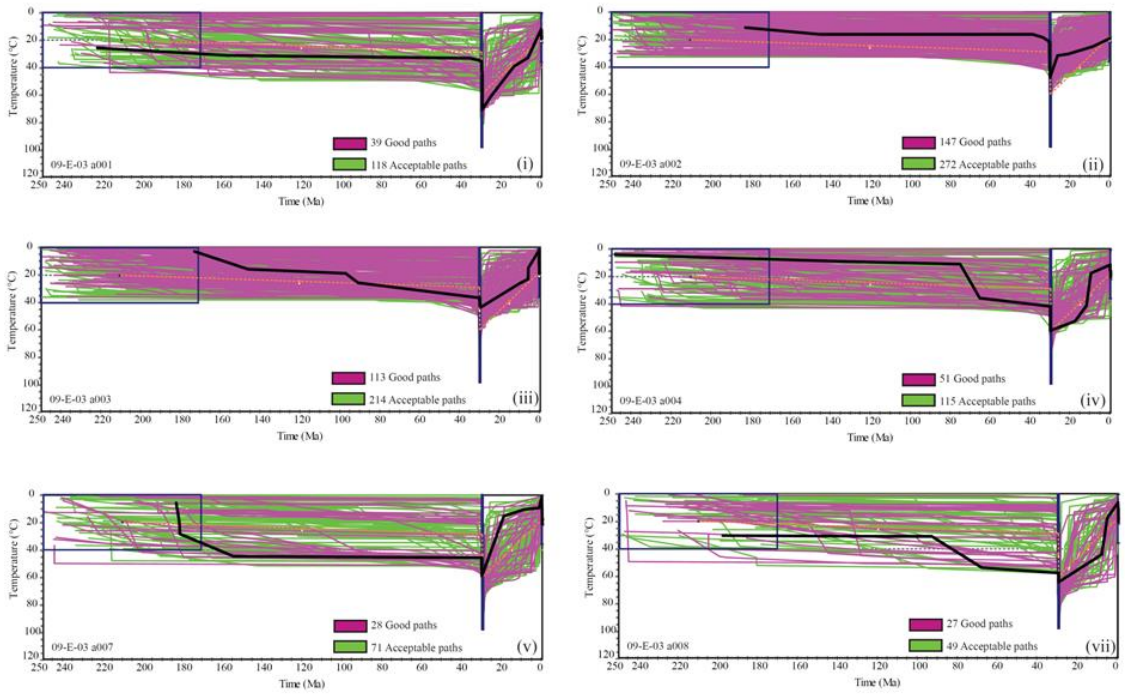

Figure 4.12: Thermal models of different apatite grains in sample 3.

CHAPTER 5: DISCUSSION

The timing of the incision of the Blue Nile Canyon on the Ethiopian Plateau is less understood as compared to the incision of the well-studied Grand Canyon in Arizona, U.S.A. This study obtained new single grain apatite (U-Th)/He dates from Neoproterozoic basement rocks and Mesozoic sedimentary rocks from the vertical transect of the Blue Nile Canyon (Figure 2.3).

All the single apatite grains were selected based on geometry, absence of inclusions, and absence of fractures. These grains yielded (U-Th)/He dates ranging from 64 Ma to 460 Ma. In general, AHe dates of a canyon incision show a clear trend of younger cooling ages with increasing depth (e.g., Schildgen et al., 2007), and the actual AHe age is interpreted to lie between the minimum AHe age and the mean AHe age (Fitzgerald et al., 2006). The AHe data of this study cannot be explained by simple age-elevation relationship, and showed significant dispersion in AHe ages, most of which are much older than AHe dates reported by Pik et al. (2003) from a nearby locality.

However, this dispersion can be explained by geologically reasonable thermal history. In this chapter, a discussion on the possible causes of data dispersion is provided relative to the results related to the diffusivity of He (e.g., Flowers et al., 2007), which is crucial for correct interpretation of AHe dates in a complex geologic history like the Ethiopian Plateau. In fact, in an area with a single thermal history, radiation damage and grain size effects on He retention can also result in wide variation in apatite (U-Th)/He dates (Flowers and Kelley, 2011). Radiation damage occurs at each step in the radioactive decay chain. Fission tracks caused by particle ejection provide avenues for enhanced He diffusion. Radiation could cause additional errors in AHe dating, such as

causing faster He diffusion in younger apatite grains. This faster He diffusion may be caused by the radiation-induced lattice defects (Farley, 2000), and these lattice defects generate nano pores of the gas to permeate. Radiation damage on He diffusivity that will produce eU-age correlation can exists due to thermal histories, such as slow cooling, longer residence time in the PRZ, and reheating due to burial or volcanism (e.g., Flowers et al., 2007).

Variable statistical methods were constructed and thermal models were generated using the (U-Th)/He dates to understand possible causes to better delineate the thermal history of the study area. The new single grain apatite dates show a distinct positive correlation with the radiogenic materials' eU (i.e., Flowers et al., 2007). Apatite grains with higher eU will accumulate more radiation damage, and hence may retain more He rather than diffusing it from grains (Shuster et al., 2006; Flowers et al., 2007; 2009; Ault et al., 2009; Shuster and Farley, 2009; Flowers and Kelley, 2011). Higher eU values, therefore, will yield older ages for similar thermal history (Flowers and Kelley, 2011). This correlation exists in most of the dates used for thermal modeling: For example, grain 2 in sample 1 has a higher eU (20.9 ppm) concentration and older age (95.46 Ma) than grain 3 in sample 3 that has a lower eU (3.78 ppm) and younger age (64.72 Ma). Despite having these eU concentration differences, these two grains share a similar thermal/cooling history with a rapid cooling event after 10 Ma. Similar dates with a wide range of eU and grain size can also characterize rapid cooling events (Flowers and Kelley, 2011), which is observed in the actual age plot where all the samples (1-5, 7, and 9) are of similar age, despite the presence of a wide range of eU concentration. These samples would have undergone rapid cooling events related to the plateau incision.

Apatite grains in basement rocks are much younger (Sample 1 has ages ranging from 58.9-176.9; sample 2, 71.7 to 120.8 Ma; sample 3, 64.7 to 132.4 Ma; sample 5, 58.9 to 227 Ma; sample 6, 109.3 to 231 Ma; and sample 7, 76.3 to 93.1 Ma) than the age of the basement rock (850 to 550 Ma) that was documented from U-Pb and Rb-Sr studies (Ayalew et al., 1990). Currently these rocks crop out at an elevation of ~700–2100 m along the Blue Nile Canyon where the Blue Nile is flowing northwest towards the low land of Sudan (Figure 2.4). The Neoproterozoic basement rocks have undergone prolonged periods of peneplanation. During this time, the apatite grains might have undergone protracted cooling at ~70°C and spent a longer time in the He PRZ. As the NW-SE trending continental rifting began in the Triassic, syn- and post-rift sedimentation followed pre-rift sedimentation until the Cretaceous. This allows accumulation of ~1.2 km thick (Gani et al., 2009) rift sedimentary rocks (including fluvial sandstones and marine limestones). The plateau gained ~1 km domal uplift related to the Afar mantle plume by the early Oligocene (Şengör, 2001). Thus, the plateau was at or near sea level before the Oligocene but, at present, the top contact of the rift sedimentary succession lies at an average elevation of 2 km (Gani et al., 2007). Sedimentary rock samples collected from the plateau include sample 8 with AHe ages of 168 Ma and 460 Ma and sample 9 with an AHe age of 96.6 Ma, which are also similar and younger than the depositional age. The extensive 30 Ma flood basalt emplacement of ~1-km thick would have caused 0.8 km of subsidence to the plateau (Gani et al., 2007) and thus partial resetting of the AHe age.

Considering the above geologic history, the Neoproterozoic basement sample might have experienced a protracted thermal/cooling history long before the incision of

the Blue Nile Canyon that started after the 30 Ma flood basalt emplacement. These samples may be introduced to partial resetting related to the rift-related burial and subsidence. This protracted thermal history might influence radiation damage accumulation and annealing, thus affecting the closure temperature of the apatite grains. Because of the accumulation of pre-incision radiation damage in these apatite grains, it may be challenging to discriminate between the old and young incision models for the Blue Nile Canyon by a simple age-elevation method.

The Ethiopian Plateau experienced extensive volcanism at ~30 Ma, which deposited >1 km-thick continental flood-basalt (Hofmann et al., 1997) followed by younger repetitive Miocene-Pliocene shield volcano building episodes and Quaternary volcanism related to the Main Ethiopian Rift (Figure 2.4). The flood volcanism would likely complicate the cooling history of the dated apatite grains by partially resetting temperatures, and by increasing geothermal gradients. During the temperature resetting episode (caused by accumulation of ~1 km thick flood basalts at ~30 Ma) of the Ethiopian Plateau, apatite grains with a lower eU (and thus with lesser radiation damage) would likely undergo more He loss yielding younger dates, while apatite grains with a higher eU (thus with more radiation damage) would likely experience less He loss, yielding older dates. Hence, Radiation Damage Accumulation and Annealing Models (RDAAM) (Flowers et al., 2009) applied to this study suggest rapid cooling and fast incision after 10 Ma. This thermal/cooling history is consistent with the previous GIS-and geochronology- based study that showed an increased incision rate around 10 and 6 Ma (Gani et al., 2007) but differs from the AHe thermochronology of Pik et al. (2003), who suggested a constant incision-rate of the Blue Nile Canyon since 29 Ma.

CHAPTER 6: CONCLUSION

This study utilized single-grain AHe cooling ages to investigate Cenozoic thermal/cooling history in light of the Blue Nile Canyon incision of the Ethiopian Plateau. The ages were obtained from apatite grains that were extracted from the Neoproterozoic basement and Triassic-Jurassic sandstone samples collected from a vertical transect of the Blue Nile Canyon.

These apatite (U-Th)/He dates show significant age dispersions ranging from 64 Ma to 460 Ma that cannot be explained with a simple age-elevation relationship. Although apatite grains were selected for dating based on geometry, shape, size, diaphaneity, and absence of inclusions and fractures, data dispersion exists in the apatite grains. A number of statistical approaches were performed to investigate any relationship of the dispersed dates with the grain size, U, Th, He, eU concentrations, and a fission-track correction factor. Most of these properties showed weak to no correlation with the AHe dates. However, these dates positively correlated with an effective uranium concentration (eU). The eU is a critical parameter to understand the radiation damage effect and He diffusivity with time in apatite grains. Although these AHe dates show a wide span in eU and grain size, apatite grains with a higher eU may accumulate more radiation damage or fission track density. Therefore, high eU apatite grains retain more He and yield a greater age than apatite grains with a low eU. Reasonable thermal history using known geologic constraints can provide valuable information in modeling these dates. Since radiation damage effect is an important factor to consider for the Ethiopian Plateau samples, this study used RDAAM (Radiation Damage Accumulation and Annealing Model) to decipher a possible thermal history.

RDAAM inverse thermal models were generated using constraints from Triassic-early Jurassic rift related sedimentation, the 30 Ma continental flood basalt events, and present-day surface position. Resulting RDAAM models provided a best fit thermal/cooling history for the Ethiopian Plateau. Samples show similar thermal/cooling history despite the data dispersion present in the samples. The best fit curve shows a rapid cooling event after 10 Ma on the Ethiopian Plateau. This thermal/cooling history is in harmony with previous studies (Gani 2015; Gani et al., 2007) that showed an increased incision rate around 10 and 6 Ma. Therefore, the rapid cooling event after ~10 Ma reflects the rapid incision of the plateau.

CHAPTER 7: REFERENCES

Adamson, D.A., Williams, M.A.J. (1987). Geological setting of Pliocene rifting and deposition in the Afar Depression of Ethiopia. *Journal of Human Evolution* 16, 597-610.

Ault, A.K., Flowers, R.M., Bowring, S.A. (2009). Phanerozoic burial and unroofing history of the western Slave craton and Wopmay orogen from apatite (U-Th)/He thermochronometry. *Earth and Planetary Science Letters* 284, 1-11.

Ayalew T., Bell, K., Moore, J.M., Parrish, R.R. (1990). U-Pb and Rb-Sr geochronology of the Western Ethiopian Shield. *Geological Society of America Bulletin* 102, 1309–1316.

Bastow, I.D., Nyblade, A.A., Stuart, G.W., Rooney, T.O., Benoit, M.H. (2008). Upper mantle seismic structure beneath the Ethiopian hotspot: Rifting at the edge of the African low velocity anomaly. *Geochemistry, Geophysics, Geosystems* 9 (12) 1-25.

Berhe, S.M., Desta, B., Nicoletti, M., Teferra, M. (1987). Geology, geochronology and geodynamic implications of the Cenozoic magmatic province in W and SE Ethiopia. *Journal of the Geological Society* 144, 213–226.

Beydoun, Z.R. (1960). Synopsis of geology of East Aden Protectorate. *21st International Geological Congress, Copenhagen 1960,* Report 21, 131-149.

Beyene, A., Abdelsalam, M. G. (2005). Tectonics of the Afar Depression: A review and synthesis. *Journal of African Earth Sciences* 41, 41-59.

Bonini M., Corti, G., Innocenti, F., Manetti, P., Mazzarini, F., Abebe, T., Pecskay, Z. (2005). Evolution of the Main Ethiopian Rift in the frame of Afar and Kenya rifts propagation. *Tectonics* 24, 1–21.

Braun, J. (2005). Quantitative Constraints on the Rate of Landform Evolution Derived from Low-Temperature Thermochronology. *Reviews in Mineralogy & Geochemistry* 58, 351-374.

Chorowicz, J. (2005). The East African Rift System. *Journal of African Earth Sciences* 43 (1-3), 379-410.

Collet, B., Taud, H., Parrot, J. F. (1999). Altimetric anomalies in the Afro-Arab zone. *Eclogae Geologicae Helvateae* 92, 275-284.

Corti, G. (2009). Continental rift evolution: From rift initiation to incipient break-up in the Main Ethiopian Rift, East Africa. *Earth-Science Reviews* 96, 1-53.

Davidson, A., Rex, D.C. (1980). Age of volcanism and rifting in southwestern Ethiopia. *Nature* 283, 657-658.

Dugda, M.T., Nyblade, A.A., Julia, J. (2007). Thin Lithosphere Beneath the Ethiopian Plateau Revealed by a Joint Inversion of Rayleigh Wave Group Velocities and Receiver Functions. *Journal of Geophysical Research* 112, B08305, 1-14.

Ebinger, C.J. (2005). Continental breakup: the East African perspective. *Astronomy and Geophysics* 46(2), 16–21.

Ebinger, C.J., Bechtel, T., Forsyth, D., Bowin, C. (1989). Effective elastic plate thickness beneath the East African and Afar plateaus and dynamic compensation of the uplifts. *Journal of Geophysical Research* 94, 2883–2901.

Ehlers, T., Farley, K. (2003). Apatite (U–Th)/He thermochronometry: methods and applications to problems in tectonic and surface processes. *Earth and Planetary Science Letters* 206, 1-14.

Farley, K.A. (2000). Helium diffusion from apatite:General behavior as illustrated by Durango fluorapatite. *Journal of Geophysical Research* 105 (B2), 2903–2914.

Farley, K.A.,Wolf, R.A., Silver, L.T. (1996). The effects of long alpha stopping distances on (U–Th)/He ages. *Geochimica et Cosmochimica Acta* 60(21), 4223– 4229.

Fitzgerald, P.G., Baldwin, S.L., Webb, L.E., O'Sullivan, P.B. (2006). Interpretation of (U-Th)/He single grain ages from slowly cooled crustal terranes: A case study from the Transantarctic Mountains of southern Victoria Land. *Chemical Geology* 225 (1-2), 91–120.

Flowers, R.M. Kelley, S.A. (2011). Interpreting data dispersion and inverted dates in apatite (U-Th)/He and fission-track datasets: An example from the U.S. midcontinent. *Geochimica et Cosmochimica Acta* 75, 5169-5186.

Flowers, R.M., Schoene, B. (2010). (U-Th)/He thermochronometry constraints on unroofing of the eastern Kaapvaal craton and significance for uplift of the southern African Plateau. *Geology* 38 (9), 827–830.

Flowers, R.M., Ketcham, R.A., Shuster, D.L., Farley, K.A. (2009). Apatite (U–Th)/He thermochronometry using a radiation damage accumulation and annealing model. *Geochimica et Cosmochimica Acta* 73 (8), 2347–2365.

Flowers, R.M., Shuster, D.L., Wernicke, B.P., Farley, K.A. (2007). Radiation damage control on apatite (U-Th)/He dates from the Grand Canyon region, Colorado Plateau. *Geology* 35, 447-450.

Gani, M. R., Gani, N. D. (2008). Tectonic Hypotheses of Human Evolution. *Geotimes* 53 (1), 34-39.

Gani, N.D. (2015). Erosion history from incision modeling and river profile morphologies: example from the Tekeze River System, Ethiopian Plateau, East Africa. *Arabian Journal of Geosciences* 8(12), 11293-11305.

Gani, N.D., Gani, M.R., Abdelsalam, M.G. (2007). Blue Nile incision on the Ethiopian Plateau: Pulsed plateau growth, Pliocene uplift, and hominin evolution. *GSA Today* 17 (9), 4-11.

Gani, N.D., Abdelsalam, M.G., Gera, S., Gani, M.R. (2009). Stratigraphic and structural evolution of the Blue Nile Basin, Northwestern Ethiopian Plateau. *Geological Journal* 44 (1), 30–56.

Gani, N.D., Van Soest, M.C., Gani, M.R., Tadesse, K., Neupane, P.C., Falster, A. (2011). *Neogene unroofing and incision of the Ethiopian Plateau constrained from apatite (U-Th)/He thermochronometry*. Abstract EP23C-0761, poster presented at the 2011 Fall Meeting, American Geophysical Union, San Francisco, CA, 5-9 December.

Garzanti, E., Ando, S., Vezzoli, G., Megid, A. A., Kammar, A. (2006). Petrology of Nile River sands (Ethiopia and Sudan): sediment budgets and erosion patterns. *Earth and Planetary Science Letters* 252, 327-341.

Green, P. F., Crowhurst, P.V., Duddy, I.R., Japsen, P., Holford, S.P. (2006). Conflicting (U-Th)/He and fission track ages in apatite: enhanced He retention, not anomalous annealing behavior. *Earth and Planetary Science Letters* 250, 407-427.

Henricksen, B.L. (1986). Reflections on drought: Ethiopia 1983-1984. *International Journal of Remote Sensing* 7(11), 1447-1451.

Hofmann, C., Courtillot, V., Feraud, G., Rochette, P., Yirgu, G., Ketefo, E., Pik, R. (1997). Timing of the Ethiopian flood basalt event and implications of Plume birth and global change. *Nature* 389, 838–841.

Ismail, E.H., Abdelsalam, M.G. (2012). Morpho-tectonic analysis of the Tekeze River and the Blue Nile drainage systems on the Northwestern Plateau, Ethiopia. *Journal of African Earth Sciences* 69, 34–47.

Keller, G.R., Prodehl, C., Mechie, J., Fuchs, K., Khan, M.A., Maguire, P.K.H, Thompson, G.A. (1994). The East African rift system in the light of KRISP 90. *Tectonophysics* 236 (1-4), 465–483.

Ketcham, R.A. (2005). Forward and Inverse Modeling of Low-Temperature Thermochronometry Data. *Reviews in Mineralogy and Geochemistry* 58 (1), 275–314.

Kieffer, B., Arndt, N., Lapierre, H., Bastien, F., Bosch, D., Pecher, A., Yirgu, G., Ayalew, D., Weis, D., Jerram, D.A., Keller, F., Meugniot, C., (2004). Flood and shield basalts from Ethiopia: Magmas from the African Superswell. *Journal of Petrology* 45, 793–834.

Lippolt, H.J., Leitz, M., Wernicke, R.S., Hagedorn, B. (1994). (Uranium+thorium)/ helium dating of apatite: experience with samples from different geochemical environments. *Chemical Geology; Isotope Geoscience* 112, 179–191.

Long, A., Rippeteau, B. (1974). Testing Contemporaneity and Averaging Radiocarbon Dates. *American Antiquity* 39 (2), 205–215.

Marty, B., Pik, R., Yirgu, G. (1996). Helium isotopic variations in Ethiopian plume lavas: Nature of magmatic sources and limit on lower mantle contribution. *Earth and Planetary Science Letters* 144, 223–237.

Mohr, P. (1962). The Ethiopian Rift System. *Bulletin of the Geophysical Observatory of Addis Ababa* 5, 33–62.

Moucha, R., Forte, A. M. (2011). Changes in African topography driven by mantle convection. *Nature Geoscience* 4, 707-712.

Pasyanos, M.E., Nyblade, A.A. (2007). A top to bottom lithospheric study of Africa and Arabia. *Tectonophysics* 444 (1–4), 27 – 44.

Philippon, M., Corti, G., Sani, F., Bonini, M., Balestrieri, M.L., Molin, P., Willingshofer E., Sokoutis D., Cloetingh S. (2014). Evolution, distribution, and characteristics of rifting in southern Ethiopia. *Tectonics* 33, 485-508.

Pik, R., Marty, B., Carignan, J., Lavé, J. (2003). Stability of the Upper Nile drainage network (Ethiopia) deduced from (U–Th)/He thermochronometry: implications for uplift and erosion of the Afar plume dome. *Earth and Planetary Science Letters* 215 (1-2), 73–88.

Pik, R., Marty, B., Carignan, J, Yirgu, G., Ayalew, T. (2008). Timing of East African Rift development in southern Ethiopia: Implication for mantle plume activity and evolution of topography. *Geology* 36 (2) 167-170.

Quade, J., Wynn, J.G. (2008). The Geology of Early Humans in the Horn of Africa. *Geological Society of America Special Paper* 446, 1-31.

Reiners, P.W. (2005). Zircon (U-Th)/He Thermochronometry. *Reviews in Mineralogy and Geochemistry* 58 (1), 151-179.

Reiners, P.W., Brandon, M.T. (2006). Using Thermochronology to Understand Orogenic Erosion. *Annual Review of Earth and Planetary Sciences* 34, 419–466.

Reiners, P. W., Farley, K. A. (2001). Influence of crystal size on apatite (U-Th)/He thermochronology: an example from the Bighorn Mountains, Wyoming. *Earth and Planetary Science Letters* 188, 413-420.

Reiners, P.W., Ehlers, T.A., Zeitler, P.K. (2005). Past, Present, and Future of Thermochronology. *Reviews in Mineralogy & Geochemistry* 58, 1-18.

Ritsema, J., van Heijst, H.J., Woodhouse, J.H. (1999). Complex shear wave velocity structure imaged beneath Africa and Iceland. *Science* 286, 1925–1928.

Rosholt, J. N. (1959). Natural radioactive disequilibrium of the uranium series. *U.S. Geological Survey Bulletin 1084-A, Contributions to Geochemistry* 1-30.

Russo, A., Assefa, G., Atnafu, B. (1994). Sedimentary evolution of the Abby River (Blue Nile) Basin, Ethiopia. *Neues Jahrbuch fu¨r Geologie und Palae¨ontologie Monatshefte* 5, 291–308.

Schildgen, T.F., Hodges, K.V., Whipple, K.X., Reiners, P.W. Pringle, M.S. (2007). Uplift of the western margin of the Andean plateau revealed from canyon incision history, southern Peru. *Geology* 35 (6), 523-526.

Şengör, A.M.C. (2001). Elevation as indicator of mantle-plume activity. *Geological Society of America Special Papers* 352, 183–225.

Shuster, D.L., Farley, K.A. (2009). The influence of artificial radiation damage and thermal annealing on helium diffusion kinetics in apatite. *Geochimica et Cosmochimica Acta* 73 (1), 183-196.

Shuster, D.L., Flowers, R.M., Farley, K.A. (2006). The influence of natural radiation damage on helium diffusion kinetics in apatite. *Earth and Planetary Science Letters* 249 (3-4), 148–161.

Spiegel, C., Kohn, B., Belton, D., Berner, Z., Gleadow, A. (2009). Apatite (U-Th-Sm)/He thermochronology of rapidly cooled samples: The effect of He implantation. *Earth and Planetary Science Letters* 285 (1-2), 105-114.

Stamps, D. S., Calais, E., Saria, E., Hartnady, C., Nocquet, J., Ebinger, C. J. Fernandes, R. M. (2008). A kinematic model for the East African Rift. *Geophysical Research Letters* 35, L05304, 1-6.

Stern, R.J., (1994). Arc assembly and continental collision in the Neoproterozoic East African orogen. *Annual Review of Earth and Planetary Sciences* 22, 319–351.

Wolf, R.A., Farley, K.A., Kass, D.M. (1998). Modeling of the temperature sensitivity of the apatite ž U – Th / r He thermochronometer. *Chemical Geology* 148, 105–114.